

Electronic Thesis and Dissertation Repository

8-11-2017 2:30 PM

Bubble Dynamics and Bed Expansion for Single-Component and Binary Gas-Solid Fluidization Systems

Bowen Han, *The University of Western Ontario*

Supervisor: Jesse Zhu, *The University of Western Ontario*

Co-Supervisor: Shahzad Barghi, *The University of Western Ontario*

A thesis submitted in partial fulfillment of the requirements for the Master of Engineering Science degree in Chemical and Biochemical Engineering

© Bowen Han 2017

Follow this and additional works at: <https://ir.lib.uwo.ca/etd>



Part of the [Complex Fluids Commons](#)

Recommended Citation

Han, Bowen, "Bubble Dynamics and Bed Expansion for Single-Component and Binary Gas-Solid Fluidization Systems" (2017). *Electronic Thesis and Dissertation Repository*. 4787.
<https://ir.lib.uwo.ca/etd/4787>

This Dissertation/Thesis is brought to you for free and open access by Scholarship@Western. It has been accepted for inclusion in Electronic Thesis and Dissertation Repository by an authorized administrator of Scholarship@Western. For more information, please contact wlsadmin@uwo.ca.

Abstract

Gas-solid fluidized beds are widely used in industrial dry coal preparation to separate waste from coal (still a primarily important energy source worldwide). It is the density difference between coal and the waste that enables the separation. Experiments were carried out in a two dimensional gas-solid fluidized bed. Filtered air at room temperature was used as the fluidizing gas, while magnetite, sand (two types) and FCC catalyst particles belonging to Geldart groups A and B were used as bed particles. Image processing and Matlab were applied for bubble size and velocity measurements. Bubble properties and bed expansion in fluidized beds of four single-component particles and binary systems were studied. Bubble size and bubble rise velocity were found to be proportional to the distance above the gas distributor and excess gas velocity. Bubble diameter is reduced by the addition of lighter and smaller particles in a binary system. In addition, a new empirical correlation for estimation of bubble diameter was proposed for single-component and binary fluidization systems. The results were in good agreement with the experimental data.

Keywords

Coal beneficiation, two-dimensional gas-solid fluidized bed, image processing, bubble size, bubble velocity, bed expansion

Acknowledgements

Foremost, I would like to express my sincerest gratitude and deepest appreciation to my supervisor Dr. Jesse Zhu for his continuous dedication to my project. Thanks for the amazing project and generous support, continuous invaluable help during this project.

The appreciation is extended to my co-supervisor Dr. Shahzad Barghi for his valuable guidance, discussion and support over the research and writing of this thesis. His professional experience solved many problems and helped throughout the project.

I would like to thank Mr. Jianzhang Wen for the assistance of experiment setup and Dr. Xiaoyang Wei and Dr. Zhijie Fu for their help in Matlab and valuable suggestions for my project. Special gratitude is given to Mr. Xiangwei Kong and Mr. Boyu Jiang for their precious help in data analysis. I also would like to take this opportunity to say thanks to my group mates: Zhi Zhang, Tang Li, Danni Bao, Tian Nan, Haolong Wang, Lin Wang, Zhehao Jing, Zhuoqing An, Yupan Yun, Yandy Zhou, Nengze Sun, Bhuiyan Mohammad, Wenjun Luo, Wei Liu, Xiliang Sun and Jiaqi Huang for their support and friendship.

The deepest gratitude goes to my parents and other family members for encouraging me to go to study here and caring about me in my life. Thank you for supporting me and being around me whenever I need you. Wish you all healthy and happy life.

Table of Content

Abstract	i
Acknowledgements.....	ii
Table of Content.....	iii
List of Figures	vi
List of Tables.....	viii
Chapter 1, Introduction and objectives	1
1.1 The importance of coal separation	1
1.2 Gas-solid fluidization technology applied in dry coal separation.....	2
1.3 Objectives	5
1.4 Thesis structure	5
Reference	7
Chapter 2 Bubble dynamics in 2-D gas-solid fluidized bed	8
2.1 Introduction.....	8
2.1.1 Bubble size.....	9
2.1.2 Bubble rise velocity	11
2.2 Experimental.....	12
2.2.1 Experimental set-up	12
2.2.2 Experimental Methods	14
2.3 Results and Discussions.....	16
2.3.1 The minimum fluidization velocity (U_{mf}).....	16
2.3.2 Bubble size distribution	18

2.3.3 Bubble size evolution.....	20
2.3.4 Comparison of bubble diameter.....	23
2.3.5 Bubble rise velocity.....	24
2.3.6 Bed expansion.....	28
2.3.7 Development of a new correlation for bubble diameter by the modification of Darton's equation.....	34
2.3.8 Estimation of the bed density.....	36
2.4 Conclusions.....	37
Nomenclature.....	39
Reference.....	41
Chapter 3 Bubble dynamics and bed expansion in binary gas-solid fluidization.....	42
3.1 Introduction.....	43
3.2 Experimental set-up and methods.....	45
3.2.1 Experimental set-up.....	45
3.2.2 Image processing.....	47
3.2.3 Bubble size.....	49
3.2.4 Bubble rising velocity.....	49
3.3 Results.....	49
3.3.1 The minimum fluidization velocity (U_{mf}).....	49
3.3.2 Bubble size evolution.....	53
3.3.3 Bubble rise velocity.....	61
3.3.4 Bed expansion.....	64

3.3.5 Bed density estimation of binary gas-solid fluidization systems.....	71
3.4 Conclusions.....	73
Nomenclature.....	75
Reference	77
Chapter 4 General conclusions	79
Reference	82
Curriculum Vitae.....	85

List of Figures

Figure 1.1 Primary energy world consumption 2015 -----	1
Figure 1.2 Primary energy regional consumption by fuel 2015-----	2
Figure 1.3 Forces acting on a single particle-----	3
Figure 1.4 The diagram of phases in a gas-solid fluidized bed-----	4
Figure 2.1 Geldart's Powder Classification-----	10
Figure 2.2. Schematic diagram of experimental equipment-----	13
Figure 2.3 Image processing procedure: (a) Original RGB image (b) Gray image (c) Binary image (d) Image with circles-----	15
Figure 2.4 Pressure drop as a function of superficial gas velocity-----	16
Figure 2.5 Bubble diameter growth as a function of bed height and bed width-----	20
Figure 2.6 Bubble diameter D_e evolution as a function of the distance above gas distributor H for varying superficial gas velocities-----	21
Figure 2.7 Bubble diameter D_e as a function of ungasged bed height H_o -----	22
Figure 2.8 Bubble diameter D_e as a function of bed height H -----	22
Figure 2.9 Bubble diameter evolution with the distance above gas distributor-----	24
Figure 2.10 Bubble rise velocity as a function of the distance above gas distributor-----	25
Figure 2.11 Bubble rise velocities of different particles-----	25
Figure 2.12 Bubble rising velocity as a function of bubble diameter-----	26
Figure 2.13 Forces acting on a single bubble-----	27
Figure 2.14 Direct observation-Bed expansion as a function of excess gas velocity-----	28
Figure 2.15 Pressure drop-Bed expansion as a function of excess gas velocity-----	29

Figure 2.16 Bed expansion e_3 as a function of excess gas velocity ($U-U_{mf}$)-----	31
Figure 2.17 Bed expansion e_4 as a function of excess gas velocity ($U-U_{mf}$)-----	33
Figure 2.18 Comparison of experimental bubble diameter and predicted bubble diameter-----	
-----	36
Figure 3.1. Schematic diagram of experimental equipment-----	46
Figure 3.2 Image processing procedure: (a) Original RGB image (b) Gray image (c) Binary image (d) Image with circles-----	48
Figure 3.3 Pressure drop as a function of superficial gas velocity-----	50
Figure 3.4 The minimum fluidization velocities of binary mixtures-----	51
Figure 3.5 Bubble size of binary mixtures as a function of the distance above gas distributor-- -----	56
Figure 3.6 Bubble size of single-component particles and binary mixtures-----	58
Figure 3.7 Bubble distribution of magnetite and binary mixture (sand 20%)-----	59
Figure 3.8 Bubble diameters calculated from equation (10) compared with experimental data-- -----	61
Figure 3.9 Bubble rise velocity as a function of the distance above gas distributor-----	63
Figure 3.10 A comparison of bubble rise velocities between mixtures and single-component particles-----	64
Figure 3.11 Bed expansion e_1 as a function of excess gas velocity-----	65
Figure 3.12 Bed expansion e_2 as a function of excess gas velocity-----	65
Figure 3.13 Bed expansion e_3 as a function of excess gas velocity-----	68
Figure 3.14 Bed expansion e_4 as a function of excess gas velocity-----	69

List of Tables

Table 2.1 Properties of particles-----	13
Table 2.2 Correlations for minimum fluidization velocity-----	18
Table 2.3 Comparison between experimental bed expansion and theoretical bed expansion---- -----	33
Table 3.1 Properties of particles and binary mixtures-----	47
Table 3.2 Correlations for minimum fluidization velocity-----	52
Table 3.3 Comparison between experimental bed expansion and theoretical bed expansion---- -----	70

Chapter 1, Introduction and objectives

1.1 The importance of coal separation

Coal is still important as a steadily available source of energy worldwide due to its vast underground resources. Figure 1.1 shows that coal's market share fell to the lowest level 29.2% in 2005, but still ranking the second largest energy source. Moreover, Figure 1.2 illustrates that coal is the dominant fuel in the Asia Pacific region, accounting for 51% of regional energy consumption - the highest share of any fuel for any region (BP Statistical Review of World Energy).

Therefore, coal cleaning technology is becoming increasingly important to produce high quality coal and reduce emission of air pollutants. In the near future, dry coal separation technology is expected to be the dominant method, replacing the traditional wet cleaning technology.

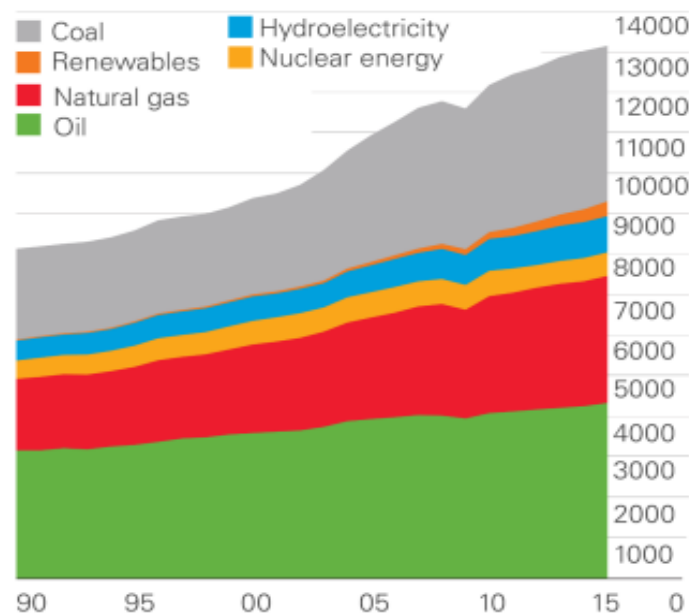


Figure 1.1 Primary energy world consumption 2015 (million tonnes oil equivalent)(BP Statistical Review of World Energy).

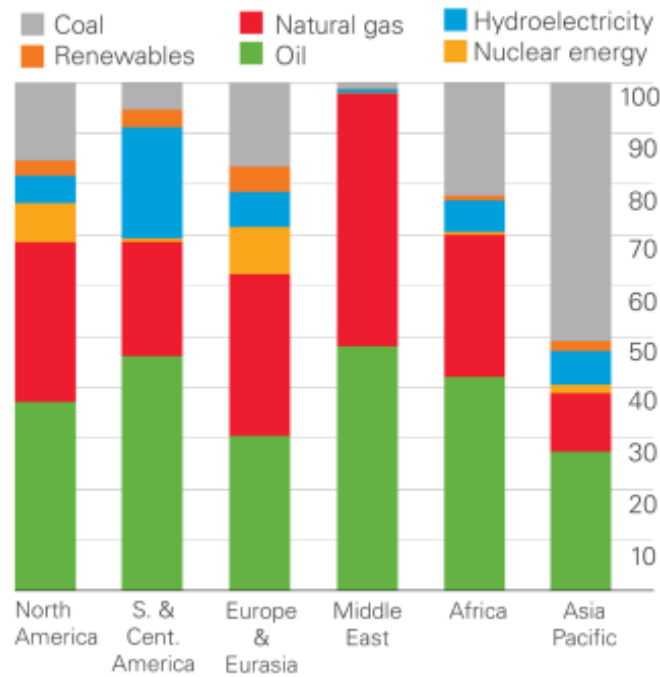


Figure 1.2 Primary energy regional consumption by fuel 2015 (percentage) (BP Statistical Review of World Energy).

1.2 Gas-solid fluidization technology applied in dry coal separation

Wet cleaning technology for coal beneficiation had been dominant for the last five decades due to its high separation efficiency (Yang et al. 2016). However, wet cleaning process requires a large quantity of water, which is becoming increasingly scarce for people living near coal mines due to serious water contamination. As an alternative method, dry coal separation technology exhibits the most important advantage over wet cleaning process-no need for water. The first fluidized bed applied for coal separation was conducted in a lab utilizing river sand as the medium solids to separate gangue from coal (Fraser and Yancey 1926). A mixture of fine magnetite powder and sand particles was also used as the fluidizing medium (Iohn 1971). The density of this mixture is lower than that of magnetite but higher than that of sand particles. Warren Spring Laboratory (1966) invented a fluidized bed with an inclined vibratory trough, using magnetite powder as the fluidizing medium in United Kingdom. Researchers

(Beeckmans and Minh 1977) at Western University (UWO) developed a counter-current fluidized bed cascade (CCFC) system to separate sand from coal. Recently, an air-dense medium-fluidized bed (ASMFB) designed at China University of Mining and Technology (1994) has been widely studied due to its high efficiency.

The fluidizing medium inside a gas-solid fluidized bed behaves like a liquid, which allows particles heavier than the medium to sink to the bottom and particles lighter than the medium to float to the surface. The Archimedes' principle perfectly explains this separation mechanism based on the analysis of various forces acting on the particles as shown in Figure 1.3.

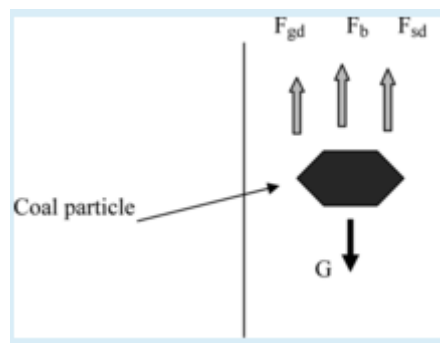


Figure 1.3 Forces acting on a single particle.

where G is the gravity force, F_b is the buoyant force, F_{gd} is the friction drag force of air and F_{sd} is the drag force of dense medium.

The density difference between medium solids and feed particles enables this physical gravity separation. Therefore, the density of the medium solids plays a vital role in the separation process. Moreover, the uniformity of bed density can ensure a high separation efficiency, which is difficult to achieve due to the non-uniformity of bed density caused by bubbles.

Based on the two-phase theory of gas-solid fluidization shown in Figure 1.4 (Davidson and Harrison 1963), a gas-solid fluidized bed consists of dense phase and bubble phase with

significantly different properties.

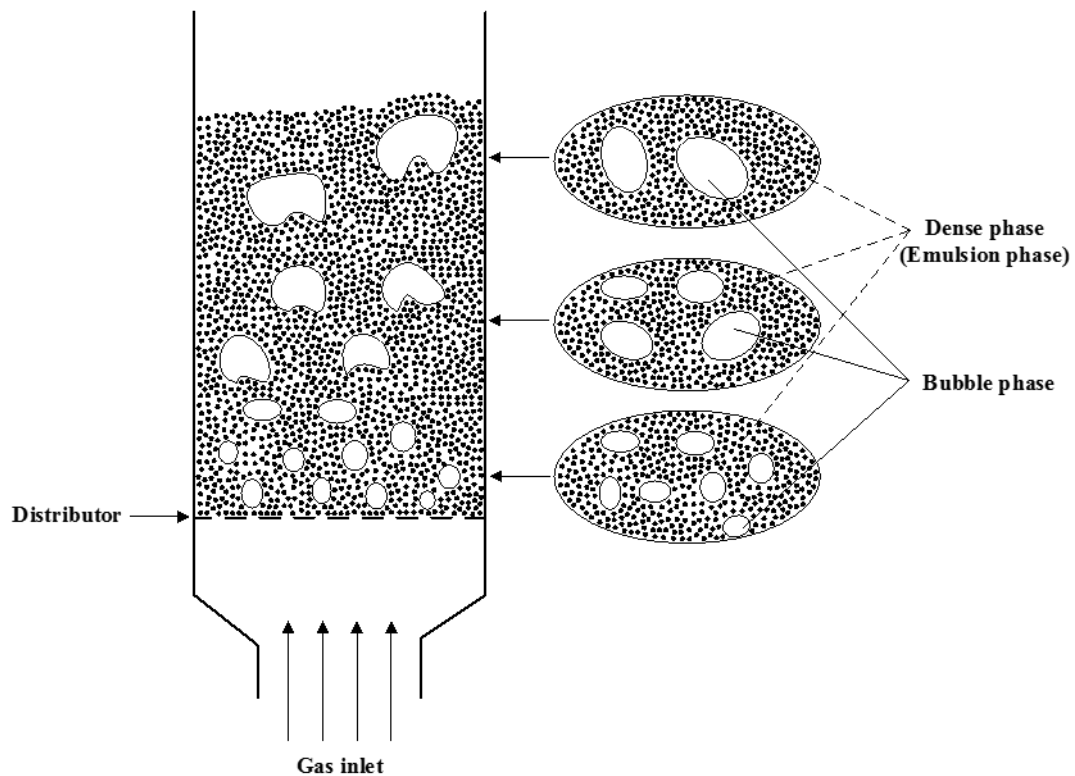


Figure 1.4 The diagram of phases in a gas-solid fluidized bed.

Bubbles inside the fluidized bed continue to rise to the surface from the gas distributor, carrying solid particles in their wake, which results in non-uniformity of the bed density. Solids mixing is crucial in coal beneficiation to ensure an efficient separation. Such mixing is induced by bubbles motion, breakage and coalescence. Particles are dragged upward in the bubbles wake while particles in the emulsion phase fall downward along the bubble walls. Particles fall in boundary layer formed around the bubble, however the irregular shape of the bubbles make it difficult to accurately determine the particles flow quantitatively. Study of particles micro-mixing which is related to boundary layer and interaction between the gas and particles as well as bubble wake phenomenon is quite challenging and out of scope of this study.

The medium solids usually are comprised of single-component particles with higher density to proceed the separation, which significantly affects the range of choices of feed coal. In order to lower the density of medium solids, binary mixtures of particles were introduced.

1.3 Objectives

Corresponding to the non-uniformity of bed density, the bubble behavior in a two-dimensional gas-solid fluidized bed using different particles is of main concern in this study, aimed to reach the following objectives:

- The relationship between bubble size and particle type, particle size, ungassed bed height and distance above gas distributor.
- The variation of bubble size and bubble velocity at different operating conditions.
- A new correlation for estimation of bubble diameter for single-component and binary fluidization systems.
- Develop a method to determine the bed density for single-component and binary fluidization systems.

1.4 Thesis structure

This thesis consists of four chapters and follows the ‘monograph’ format as outlined by the Master’s Programs of GENERAL THESIS REGULATIONS by the School of Graduate and Postdoctoral Studies (SGPS) at the University of Western Ontario (UWO). A summary of each chapter is provided below.

Chapter 1 consists of general introduction and literature review, including industrial applications and objectives. The development of coal cleaning technologies and studies about

bubble dynamics are elaborated.

Chapter 2 is focusing on the study of bubble properties in 2-D gas-solid fluidized beds with single-component particles. Details about experiment and image processing technology are provided.

Chapter 3 reports the bubble dynamics in 2-D gas-solid fluidized bed with binary mixtures.

The variation of bubble size in binary mixtures is presented.

Chapter 4 provides general conclusions. The first part is conclusions of bubble properties as a function of particle type, particles size, ungassed bed height and the height above the gas distributor. A new correlation for estimation of bubble diameter was also proposed in the first part. The second part is comprehensive studies of bubble dynamics and bed expansion in binary fluidization systems.

Reference

BP Statistical Review of World Energy 2016, BP, London 2016.

Beeckmans, J. M. and T. Minh (1977), Separation of mixed granular solids using the fluidized counter-current cascade principle, *The Canadian Journal of Chemical Engineering* 55: 493-496.

Chen Q. R. and Y. F. Yang(1994), Development of dry beneficiation of coal in China, *Coal preparation* 23: 3-12.

Douglas, E. and T. Walsh (1966), New type of dry heavy medium gravity separator, *Transactions of the Institute of Mining and Metallurgy* 75C: 226–232.

Davidson, J. F. and D. Harrison (1963), *Fluidized particles*, Cambridge university press.

Fraser, J. and H. F. Yancey (1926), Artificial storm of air-sand floats coal on its upper surface, leaving refuse to sink, *Coal Age* 29: 325-327.

Lohn, P. (1971), Fluidized bed heavy medium separation-A modern dry separation procedure, *Aufbereitung Technik* 3: 140-146.

Xuliang Yang, Yuemin Zhao and Zhenfu Luo (2016), Dry cleaning of fine coal based on gas-solid two-phase flow: A review, *Chemical Engineering Technology* 40(3): 439-449.

Chapter 2 Bubble dynamics in 2-D gas-solid fluidized bed

2.1 Introduction

Gas-solid fluidization technology has been widely used in different processes, such as fluid catalytic cracking, fluidized bed combustion, coating and dry coal separation. Among these applications, dry coal beneficiation exhibits remarkable advantages over wet cleaning technology, such as no need for water, less air pollution, no slurry treatment and so on (Dwari and Rao 2007, Houwelingen and Jong 2004). Density difference as the basic principle perfectly explains this physical separation. Particles relatively heavier than the bed medium sink towards the bottom of the bed, while particles lighter than the bed float to the bed surface (Sahu, Biswal and Parida 2009). Bubble behaviour has a significant effect on the mass transfer, heat transfer, bed density and chemical reactions. Therefore, knowledge of bubble dynamics is essential for improving efficiency of gas-solid fluidized bed for industrial applications. Various measurement systems have been developed to determine the bubble properties in fluidized beds, including different probes and photography. Several probe measurement systems, belonging to intrusive measurement technologies, have been utilized in recent years, which includes needle type capacitance probes (Werther and Molerus 1973), optical probes (Yasui and Johnson 1958, Andreux and Chaouki 2005) and electro-resistivity and conductivity probes (Park and Kang 1969). Photography technologies belonging to non-intrusive measurement technologies, are mainly composed of direct photography (Geldart 1970), X-ray photography (Rowe and Partridge 1965) and electrical capacitance tomography (Halow, Fasching, Nicoletti and Spenik 1993, McKeen and Pugsley 2003).

In the last decade, investigations of bubble characteristics have been carried out using image

analysis technology. However, almost all of these studies used lights placed at the back of the fluidized bed, while a camera was placed at front. In this case, fewer bubbles were observed due to the thickness of the bed. Another issue caused by the thickness is that particles surrounding bubbles may decrease the visibility of the bubbles. 2D fluidized beds, overcoming these shortcomings, have been widely used for investigations of bubble behavior in recent years.

In this study, experiments for investigation of bubble properties in a two dimensional gas-solid fluidized bed were conducted. The behaviour of bubbles was recorded and processed using image processing technology. The objective of this work is to get bubble distribution, bed expansion and bubble parameters as a function of the height, particle size, particle type, and superficial gas velocity using image analysis.

2.1.1 Bubble size

When particles in a fluidized bed are fluidized by an upward flow of gas, bubbles are formed by excess gas (the superficial gas velocity exceeding the minimum fluidization velocity).

Bubbles generated at the bottom rise through the bed to the surface. During this process, bubbles continually coalesce and break up reaching a balance between them and evolve at varying bubble diameter (Horio and Nonaka 1987).

Yasui and Johanson (1958) made the first attempt to study bubble dynamics in fluidized beds using 4-in and 6-in columns. They derived an empirical correlation for predicting bubble diameter from the experimental data directly measured using the light probe technique. Five different particles ranging from 12 μm to 450 μm were used. Lim et al. (1990) were the first

researchers who utilized image analysis technology to study bubble characteristics. Geldart (1970) derived another formula of bubble size in a 3D bed from data collected from a 2D bed. A transition of bubble diameter from 2D bed to 3D bed is needed, because their flow dynamics are different (Ma, Liu and Chen 2015). Mori and Wen (1975) proposed a correlation of bubble diameter and growth in fluidized beds. Furthermore, the bubble diameters calculated from this correlation are in good agreement with the bubble sizes observed. Darton's equation (Darton et al. 1977) for bubble diameter has been the most widely used by researchers due to its good coverage under all conditions. However, this correlation excluded mechanism of bubbles splitting and breakage. Therefore, a continuously increasing pattern of bubble diameter was obtained from their work (Karimipour and Pugsley 2011). However, in real cases, bubbles splitting and coalescence do exist and are of critical importance for bubble size evolution. Horio and Wen (1977) pointed out that the equilibrium bubble size should be the result of a balance between bubble coalescence and break up. For the cases of group A particles (Geldart 1973, shown in Figure 2.1), splitting and breakage occur in a high frequency in a fluidized bed of group A particles, which implies that the correlation of Darton cannot provide the best coverage for group A particles.

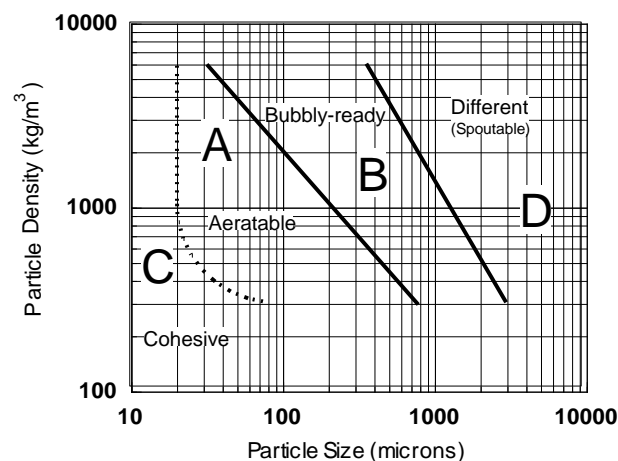


Figure 2.1 Geldart's Powder Classification.

Busciglio and Vella (2010) performed the investigation on bubble size distribution in a 2D fluidized bed by means of image analysis technology. The same technology was also employed by Ma et al. (2015) to study bubble behavior of large cohesive particles in a 2D fluidized bed.

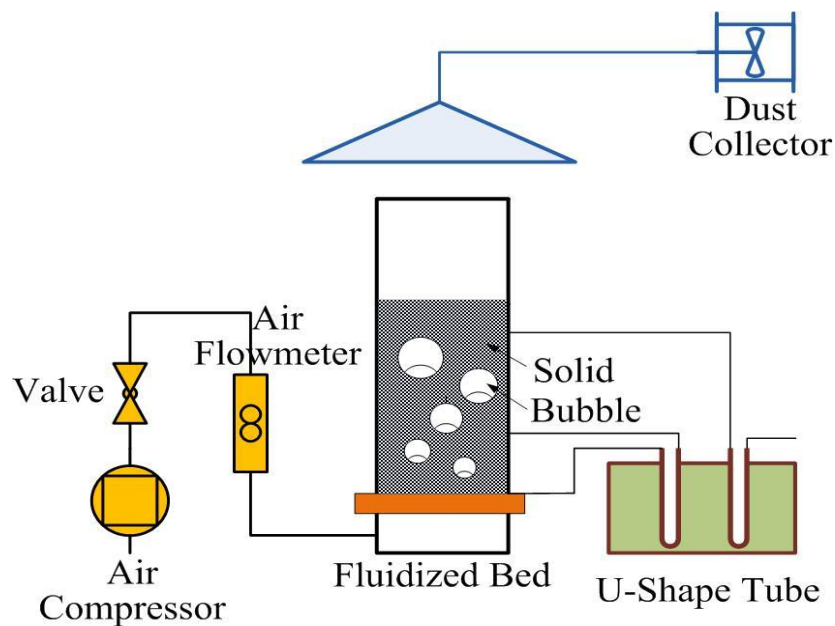
2.1.2 Bubble rise velocity

In recent years, compared to bubble size, fewer studies of bubble velocity have been conducted by researchers. Davidson and Harrison (1963) developed the most widely used equation for bubble velocity. Corresponding to this correlation, bubble rise velocity is dominated by the bubble diameter. Another factor contributing to bubble velocity is the excess gas velocity. Whitehead et al. (1967) measured the bubble rise velocity using an optical probe in a 10 cm squared fluidized bed filled up with silica sands at varying excess gas velocities. They found that average bubble velocity is proportional to the excess gas velocity and bubbles rose faster in fine sand. Werther (1974) reported the existence of a maximum bubble rise velocity in several cylinder beds using a needle capacitance probe. Verma et al. (2014) investigated bubble rise velocity in a 3D fluidized bed with glass, alumina and low linear density polyethylene (LLDPE) using X-ray tomography technology. The experimental results of their work showed a good agreement with the simulations. They also found that the LLDPE particles have higher bubble rise velocity compared to the data calculated from previous correlations.

2.2 Experimental

2.2.1 Experimental set-up

Figure 2.2 shows the schematic diagram of the experimental setup. The fluidized bed designed for present study on bubble dynamics is made of Perspex (1500 mm height, 370 mm width and thickness of 19 mm), which provides detail observation of bubble behaviors inside the bed. There are three pressure measurement ports along the bed wall located at bed height of 0 mm, 180 mm and 550 mm. Two lights were placed in front of the fluidized bed to enhance the contrast between the bubble and dense phases, allowing more small bubbles being visualized. The bubble behaviors were recorded by a digital camera (Canon T3i), which was placed on the opposite side of the bed. All videos were recorded at the steady state condition (complete fluidization).



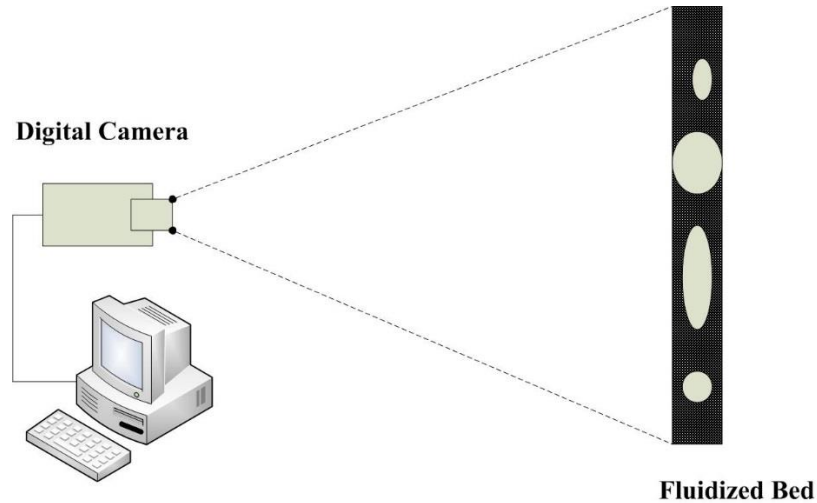


Figure 2.2. Schematic diagram of experimental equipment.

A sintered plastic gas distributor placed at the bottom of fluidized bed is designed with 10 micron holes. Below the gas distributor is the wind box used to ensure uniform distribution of inlet gas across the distributor. Air was used as the fluidizing gas and controlled by three air rotameters ranging from 0 m³/h to 5 m³/h.

Four types of particles were used at bed heights of 300 mm, 450 mm and 600 mm in the fluidized bed. Particles were fluidized by the upward air at varying superficial gas velocities.

The excess gas velocities (defined as the difference between superficial gas velocity and minimum fluidization velocity) were kept constant at 1.63 cm/s, 4.37 cm/s and 7.05 cm/s.

Other characteristics of particles have been summarized in Table 2.1. Geldart A particles and Geldart B particles were used in the experiments, to cover a wider range of particles.

Table 2.1 Properties of particles

Particle type	ρ_p (kg/m ³)	d_p (μ m)	Geldart type
Magnetite	4650	150-300	B
Sand	2650	150-300	B

Sand	2650	75-125	A/B
FCC catalyst	1540	75-125	A

2.2.2 Experimental Methods

2.2.2.1 Image processing

The bubble behavior in the fluidized bed was videotaped after steady state condition was reached. The camera employed recorded video at a frequency of 29 Hz, which implies 29 frames per second. Each frame is a 1088 X 1920 pixel picture. The pixel ranging from 0 to 255 is called grey-value which indicates brightness. Grey-value 0 is black while grey-value 255 means white. Each position in the picture has its own grey-value. In this way, pictures are transferred to a matrix, which can be analyzed using MATLAB (Matrix Laboratory).

The experimental procedure for image processing can be summarized into several steps : 1. Split the video into consecutive frames. 2. Transfer original RGB images into grey images. 3. Set a threshold to transfer grey images into binary images. 4. Do the subtraction of grey-value between fluidizing particles images and ungasped particles image to determine bubble properties. 5. Depict the contour of bubbles and obtain bubble characteristics applying a package of software ‘Regionprops’. A video used as the base was recorded before air was introduced into bed. Then grey-value’s difference between the base image and fluidizing images of every position was obtained. A non-zero grey-value difference implies a position where bubble exists due to different grey-values between dense phase and bubble phase.

Figure 2.3 shows the images used in the analysis.

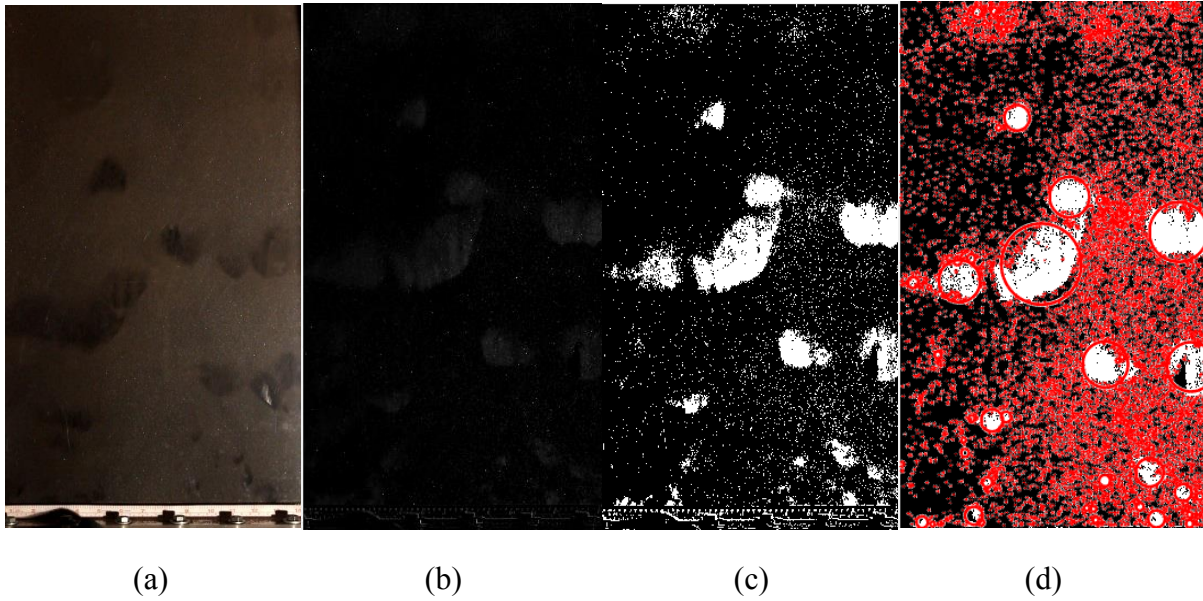


Figure 2.3 Image processing procedure: (a) Original RGB image (b) Grey image (c) Binary image (d) Image with circles

2.2.2.2 Bubble size

The bubble phase was discriminated from the dense phase based on grey-value difference.

However, a threshold needs to be determined to improve the discrimination between these

two phases because of the disturb of noise points. In this study, the threshold was determined

to be 10 to exclude the impact of noise points. The area of a bubble (A_b) is the number of

pixels forming this bubble. Every single bubble was transformed into a circle with the same

area using a software called Regionprops. According to the bubble area, the equivalent

bubble diameter D_e can be calculated from the following equation:

$$D_e = 2 \sqrt{\frac{A_b}{\pi}} \quad (1)$$

2.2.2.3 Bubble rise velocity

The camera applied in this investigation recorded videos of 29 frames per second. Therefore,

the time interval (Δt) between every two consecutive frames is 1/29 second. The coordinates

(x_i, y_i) of the bubble center in each frame can be determined automatically by the means of image processing technology. In this way, the axial distance $(y_i - y_{i-1})$ that every single bubble moves between every two consecutive frames was obtained. Then the bubble rising velocity can be calculated from the following equation:

$$u_b = \frac{y_i - y_{i-1}}{\Delta t} \quad (2)$$

2.3 Results and Discussions

2.3.1 The minimum fluidization velocity (U_{mf})

The minimum fluidization velocity is the fluid velocity at incipient fluidization of a packed bed filled up with particles. It is a critical variable for designing fluidized beds. In this work, the minimum fluidization velocity (U_{mf}) is determined by measuring the pressure drop as a function of superficial gas velocity (shown in Figure 2.3).

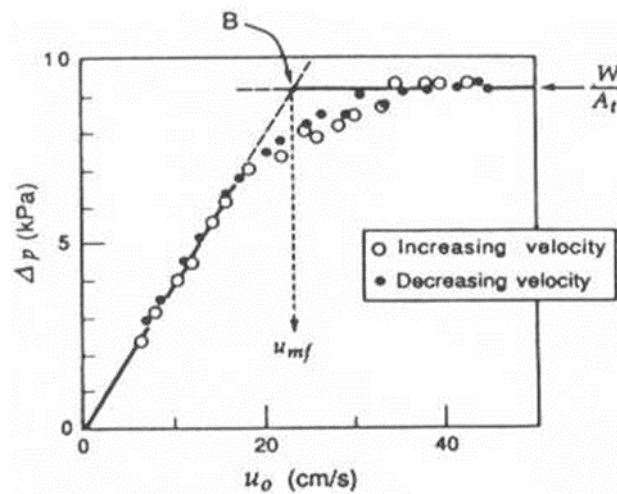


Figure 2.4 Pressure drop as a function of superficial gas velocity.

Pressure drop remains almost constant after superficial gas velocity exceeds certain value.

This value is determined as the minimum fluidization velocity, at which the particles inside the bed begin to be fluidized. Many correlations for predicting minimum fluidization velocity

have been reported, such as correlations of Narsimhan (1965), Wen and Yu (1966) and Coltters and Rivas (2004). The equation of Wen and Yu for the minimum fluidization velocity is described as follows:

$$A_r = 24.5Re_{mf}^2 + 1650Re_{mf} \quad (3)$$

where

$$A_r = d^3 \rho_g (\rho_p - \rho_g) \frac{g}{\mu^2} \quad (4)$$

$$Re_{mf} = \frac{d \rho_g u_{mf}}{\mu} \quad (5)$$

The correlation of Coltters and Rivas for the minimum fluidization velocity is given by

$$U_{mf} = KX^\alpha \quad (6)$$

where

$$X = \frac{d^2 (\rho_p - \rho_g) g}{\mu} \left(\frac{\rho_f}{\rho_g} \right)^{1.23} \quad (7)$$

For metallic ores-gas fluidizing system $101\mu\text{m} < d < 1250\mu\text{m}$

$$K = 3.1108 \times 10^{-8}, \alpha = 0.93283 \pm 0.03451$$

For sand-gas fluidizing system $95\mu\text{m} < d < 800\mu\text{m}$

$$K = 9.7119 \times 10^{-7}, \alpha = 0.84268 \pm 0.01601$$

For catalyst-gas fluidizing system $25\mu\text{m} < d < 2250\mu\text{m}$

$$K = 1.145 \times 10^{-5}, \alpha = 0.71957 \pm 0.01422$$

where ρ_p is the density of fluid medium, ρ_g is the density of fluidizing gas, μ is the viscosity of fluidizing gas, K and α are constants.

According to these correlations, the minimum fluidization velocity depends on particle and gas properties, such as densities of solid and gas, sphericity, particle diameter, and voidage at U_{mf} (Coltters and Rivas 2004). A comparison between U_{mf} of these correlations and

experimental U_{mf} is shown in Table 2.2.

Table 2.2 Correlations for minimum fluidization velocity

Particles	d_p (μm)	ρ (kg/m^3)	Geldart type	U_{mf} predicted (cm/s)		This work
				Wen/Yu	Coltters/Rivas	Experiment
Magnetite	150-300	4650	B	7.73	6.49	10.6
Sand	150-300	2650	B	4.40	4.72	3.71
Sand	75-125	2650	A/B	0.87	1.20	1.20
FCC catalyst	75-125	1540	A	0.51	0.76	0.51

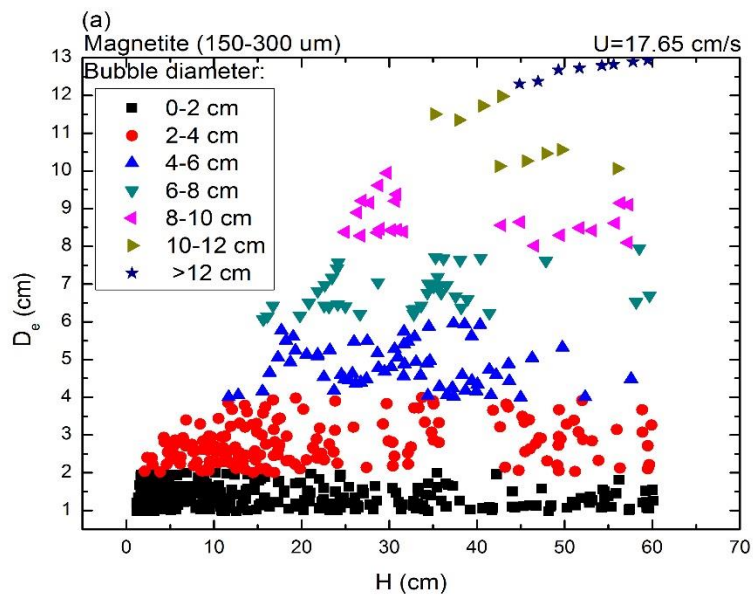
Table 2.2 shows that magnetite powder has the largest U_{mf} , while FCC catalyst has the smallest U_{mf} , which implies that FCC catalyst and sand with smaller particle size can be fluidized easier than magnetite powder and sand with larger particle size. The experimental minimum fluidization velocity has a good agreement with the results calculated from correlations in literature.

2.3.2 Bubble size distribution

Bubble size growth as a function of the bed height above the gas distributor and bed width are shown in Figure 2.5. It is clear that bubble diameter for Geldart B particles is increasing with increasing bed height. Small bubbles covers the whole bed area while large bubbles only exist in higher locations in the bed. However, in higher levels, population of small bubbles is smaller compared to that in lower levels. Figure 2.5 (a) shows that small bubbles exist at all elevations and lower region tends to have more small bubbles compared to higher region.

Figure 2.5 (b) illustrates that large bubbles exist in the central region, while small bubbles spread out along the bed width. The whole pattern of Figure 2.5 (b) acts like a triangle which means bubbles are moving toward to the center and becoming bigger due to the coalescence in the central region.

According to Figure 2.5 (a), the present trend with a large slope implies that bubble coalescence tends to occur in the central region at the elevation between 15cm and 45cm, where small bubbles assemble. After coalescence, bubbles also grow gradually due to the decreasing hydrostatic bed pressure. Therefore, bubble coalescence is the main reason for bubble growth.



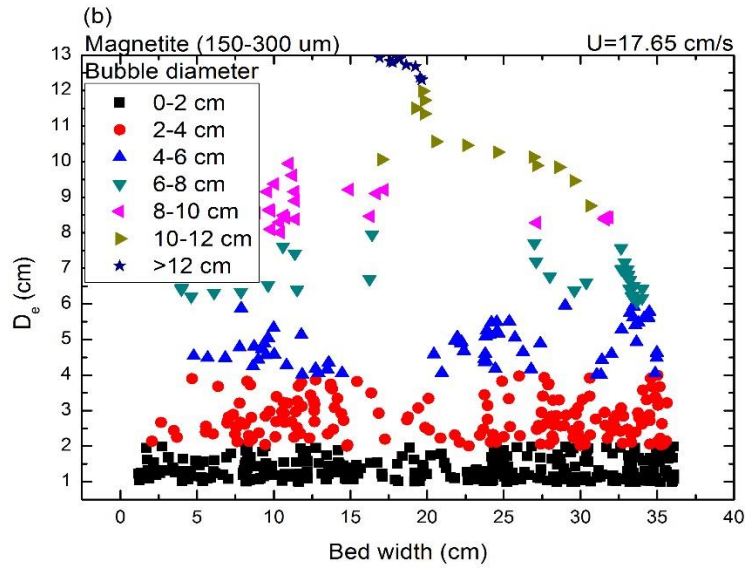


Figure 2.5 Bubble diameter growth as a function of bed height and bed width.

2.3.3 Bubble size evolution

Figure 2.6 (a) shows a remarkable increase in bubble diameter with increasing bed height at different gas velocities, while Figure 2.6 (b) shows a constant of bubble diameter for FCC catalyst at higher regions. It is attributed to small particles, which give bubbles more chance to break up. It is assumed that no bubble coalescence occurs at very high elevation due to long distances between bubbles. A balance is reached between the breakage of bubbles and the decreased bed hydrostatic pressure. For Geldart B type particles, bubbles coalesce as they rise through the whole bed, which makes bubbles grow bigger at higher elevation. These two Figures also show that bubble size increases when higher gas velocity is introduced. In addition, a sharper increase of bubble diameter is clearly observed with a higher gas velocity. It is likely due to more gas at higher gas velocity, which indicates bubbles have more chance to coalesce.

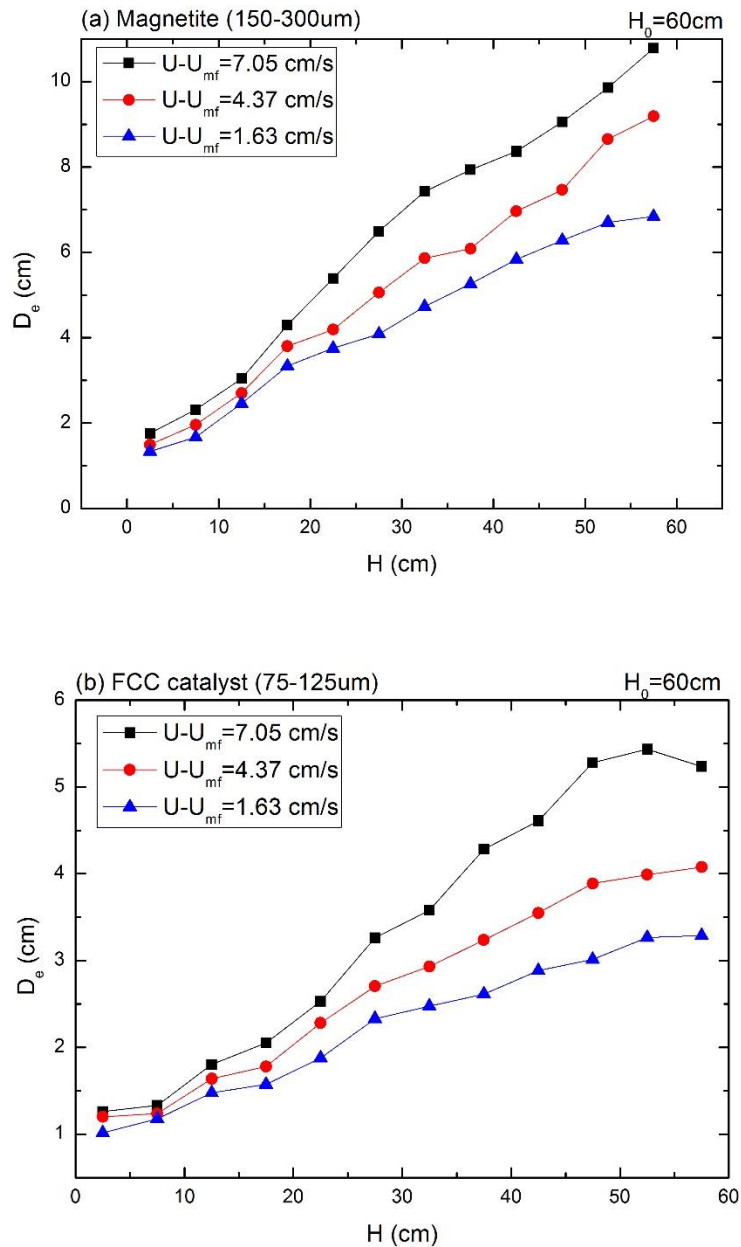


Figure 2.6 Bubble diameter D_e evolution as a function of the distance above gas distributor H for varying superficial gas velocities

Figure 2.7 illustrates that there is a decrease of bubble diameter with increasing initial bed height in lower region due to high hydrostatic pressure. In Figure 2.7, FCC catalyst (75-125 μm) with ungasged bed height of 60 cm has a constant value at the end. The bubbles have not reached the maximum size until 48 cm. Moreover, it is observed that higher initial bed height gives bubbles more space to grow larger.

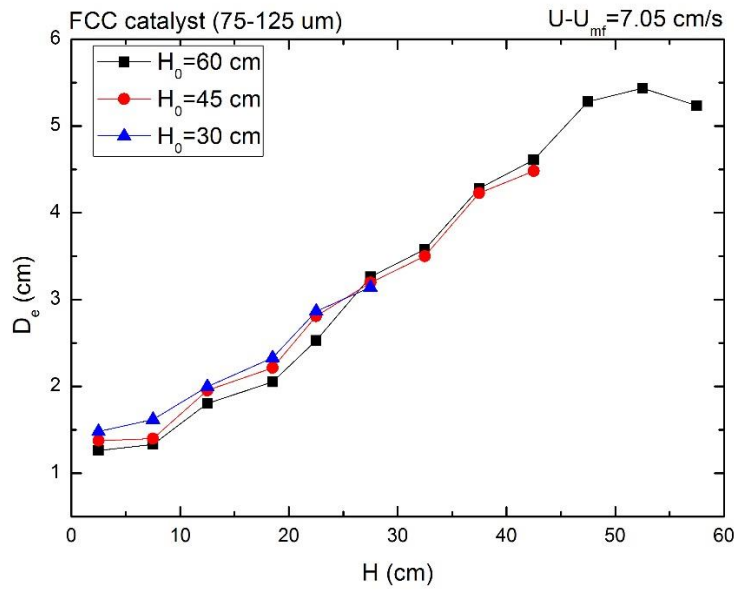


Figure 2.7 Bubble diameter D_e as a function of ungasged bed height H_0 .

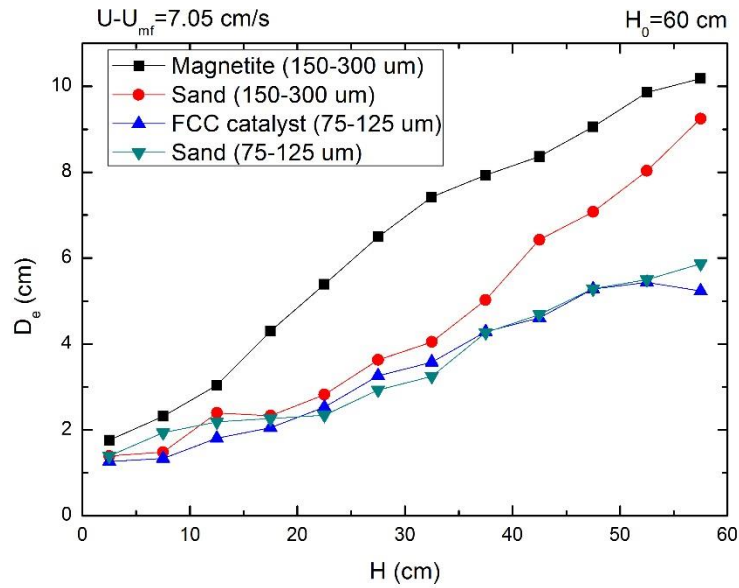


Figure 2.8 Bubble diameter D_e as a function of bed height H

Figure 2.8 shows that Geldart B type particles have bigger bubble size than Geldart A type particles. In addition, particles with larger size tend to have larger bubble size than smaller particles. This result are in good agreement with the research of Park et al. (1969) and Yasui, Johanson (1958). The voidage between Geldart B type particles is larger than that of Geldart

A type particles due to the large particle size, which means more space for the gas to form large bubbles between particles. However, the optimal fluidization should have large quantity of small bubbles homogeneously distributed in the bed (Lim et al. 2007). Base on this theory, fine particles have a better fluidization when the particles are fully fluidized. Compared to the bubble size of sand particles (150-300 μm), magnetite powder has a bigger bubble diameter due to its relatively higher density. The fluidizing gas supports the weight of particles in the whole bed when particles are fluidized. In this case, fluidizing gas in magnetite powder is easier to accumulate and forms bigger bubbles.

2.3.4 Comparison of bubble diameter

Figure 2.9 shows that the experimental bubble diameters are not in good agreement with results calculated from the correlation of Darton. Bubble diameter from Darton's equation is clearly smaller than actual bubble size. The equation of Darton et al. is described as follows:

$$D_e = 0.54g^{-0.2}(U - U_{mf})^{0.4}(h + 4A_D^{0.5})^{0.8} \quad (8)$$

According to this equation, particle properties do not have any effect on the bubble size.

However, as shown earlier, bubble diameter depends on particle size and type. Therefore, a new correlation was developed to modify Darton's correlation.

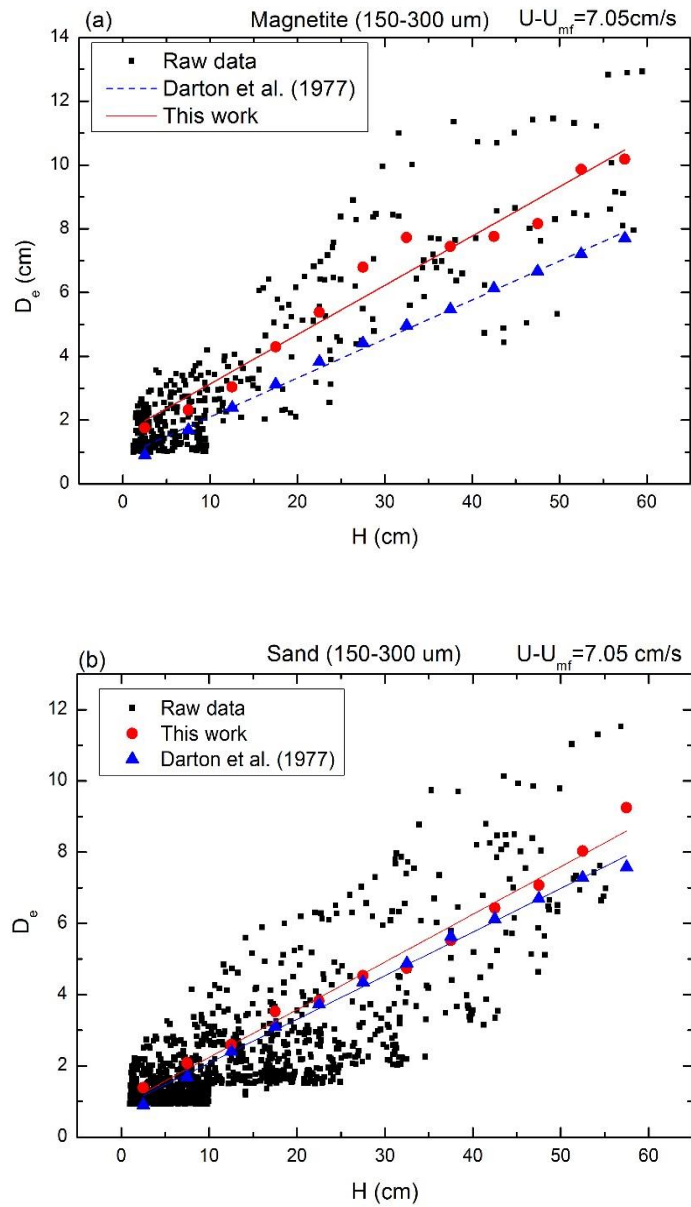


Figure 2.9 Bubble diameter evolution with the distance above gas distributor

2.3.5 Bubble rise velocity

Bubble rise velocity changes with bubble size as bubbles rise through fluidized bed. The bubble rise velocity can be determined based on bubble diameter and excess gas velocity (Davidson and Harrison 1963). The correlation of Davidson and Harrison is given by;

$$u_b = 0.71\sqrt{gD_e} + (U - U_{mf}) \quad (9)$$

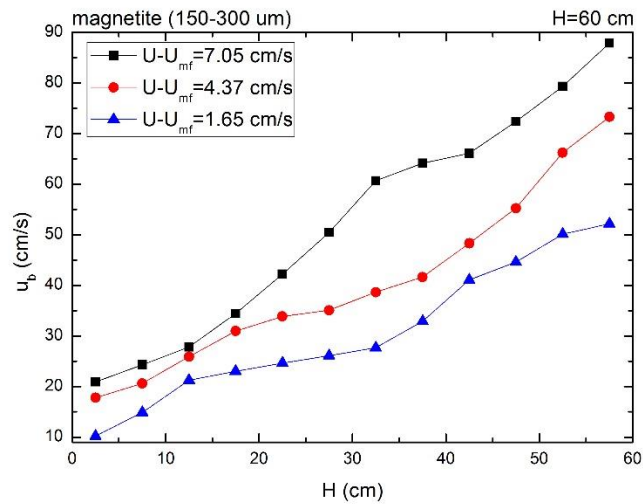


Figure 2.10 Bubble rise velocity as a function of the distance above gas distributor

Figure 2.10 clearly shows that bubble rise velocity of magnetite powder is increasing with increasing bed height and excess gas velocity. The increasing bubble rise velocity with bed height is due to the appreciable coalescence of bubbles as they rise through the bed, which makes bubbles grow larger and rise faster. The excess gas needs to get out of the fluidized dense phase in the form of bubbles. According to the mass balance of gas, larger excess gas velocity leads to larger bubble rise velocity.

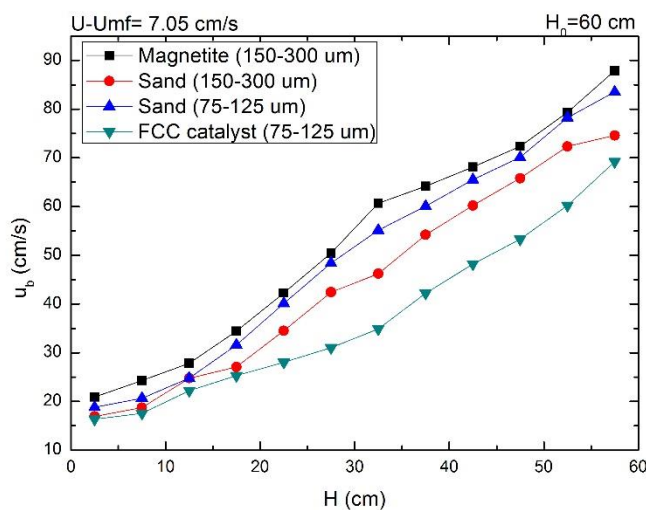


Figure 2.11 Bubble rise velocities of different particles

Figure 2.11 illustrates that magnetite powder has the largest bubble rise velocity while FCC catalyst has the smallest bubble rise velocity, which is in good agreement with the bubble diameter. However, bubble rise velocity is increasing with decreasing particle size of sand, which is in contradiction with the growth pattern of bubble size of sand. Whitehead et al. (1967) measured the bubble rise velocity using an optical probe in a 10 cm squared fluidized bed filled up with silica sands at varying excess gas velocities. They found that average bubble velocity is proportional to the excess velocity and bubbles rose faster in fine sand. In addition, Rowe and Yacono (1976) also found that bubble rise velocity increased with decreasing particles size. The reason for this phenomenon is still unknown.

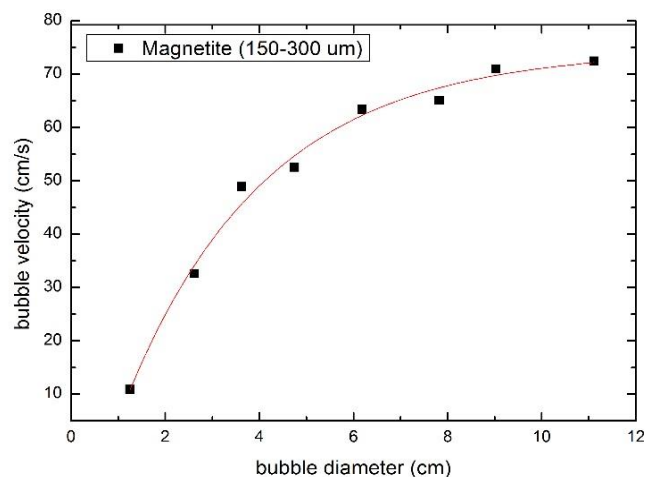


Figure 2.12 Bubble rising velocity as a function of bubble diameter

Figure 2.12 illustrates that bubble size can accelerate the bubble rising velocity, which means larger bubbles move much faster than small bubbles. Figure 2.13 shows the forces exerting on a single bubble.

The buoyant force:

$$F_b = \rho_f V_b g \quad (10)$$

where

$$V_b = \frac{1}{6}\pi D^3 \quad (11)$$

The drag force:

$$F_d = \frac{1}{2}\rho_f u^2 C_D A \quad (12)$$

where

$$A = \frac{1}{4}\pi D^2 \quad (13)$$

The gravity force:

$$G = \rho_{air} V_b g \quad (14)$$

Where ρ_f is density of the fluid, D is the diameter of bubble, u is the velocity of fluid, C_D is the drag coefficient, A is the projected surface area. The gravity force of bubble is so small that it is neglected in the following calculation.

It is clearly seen that $F_b \propto D^3$ and $F_d \propto D^2$. Therefore the ratio of buoyant force and drag force is $\frac{F_b}{F_d} \propto D$, which indicates bigger upward force with larger bubbles. Therefore, large bubbles rise faster than small bubbles.

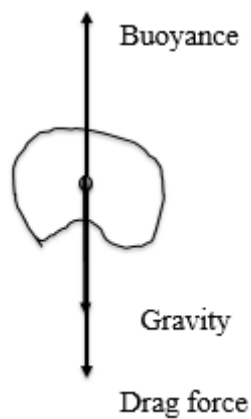


Figure 2.13 Forces acting on a single bubble

2.3.6 Bed expansion

2.3.6.1 Experimental

The bed surface is forced up to a higher level when particles inside the bed are fluidized due to additional volume occupied by the bubbles. Therefore, bed expansion is of critical importance to determine the amount of solid and gas bubbles. In this work, two methods were applied to measure bed expansion. One method is direct observation of expanded bed height, while the other is through the measurement of pressure drop. Ten pictures were taken during the first method to obtain average expanded bed height (H_e) with known initial bed height (H_0). Then the bed expansion can be calculated based on following formula:

$$e = \frac{H_e - H_0}{H_0} \quad (15)$$

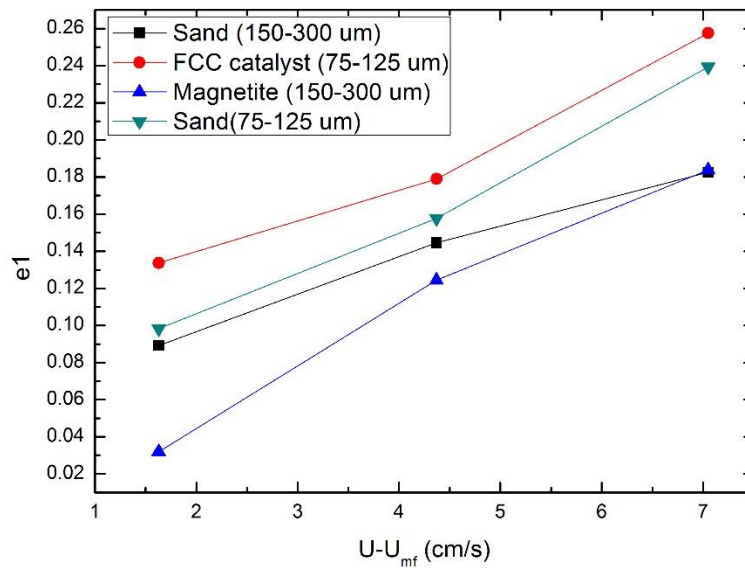


Figure 2.14 Direct observation-Bed expansion as a function of excess gas velocity

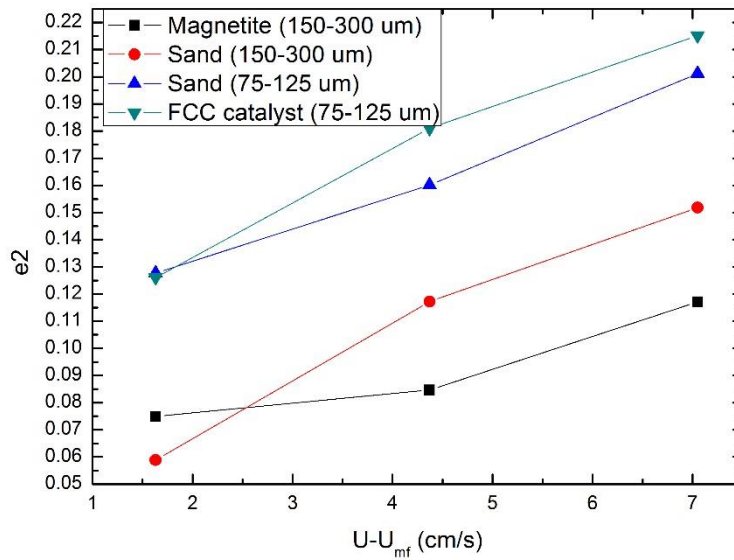


Figure 2.15 Pressure drop-Bed expansion as a function of excess gas velocity

It is observed that bed expansion increases with increasing excess gas velocity $U-U_{mf}$ due to more gas bubbles as shown in Figure 2.14 and Figure 2.15. They also show that sand with larger particle size has a bigger bed expansion than sand with smaller particle size, which indicates particles with smaller size give larger bed expansion. Moreover, these two Figures illustrate that FCC catalyst has the biggest bed expansion. Both FCC catalyst and sand (75-125 μm) belong to Geldart A type particles. According to the results, Geldart A type of particle tends to have large bed expansions, which is attributed to the large amount of small bubbles of Geldart A type of particle.

2.4.6.2 Theoretical

Bubbles grow bigger and move faster when they rise through the fluidized bed. Therefore, there are specific bubble size and bubble rise velocity at each position. An iteration method was used to obtain expanded bed height. The fluidized bed was divided into equally spaced sections with

a height of H_i . Each part has its own serial number “n”. Bubble diameter d_i and bubble velocity v_i in each part can be calculated using bubble size equation of Darton (1967) and bubble velocity equation of Davidson and Harrison (1963).

Based on mass balance on the gas phase, the number of bubbles in each part can be obtained using the following equations:

$$D_e = \emptyset(U - U_{mf})^{0.204} \left(\frac{H_i}{2} + (n - 1)H_i + 4A_D^{0.5} \right)^{0.759} / 1.2 \quad (16)$$

A single bubble volume will be:

$$V_{bi} = \frac{1}{4}\pi D_i^2 w \quad (17)$$

Then the bubble rising velocity will be:

$$u_{bi} = 0.71\sqrt{gD_i} + U - U_{mf} \quad (18)$$

The time bubble stays in each part will be:

$$t = \frac{H_i}{u_{bi}} \quad (19)$$

Then the number of bubbles in each part will be:

$$n_i = \frac{(U_g - U_{mf})t}{V_b} \quad (20)$$

and the dense phase volume will be:

$$V_{di} = AH_i - n_i V_{bi} \quad (21)$$

The summation of each dense phase volume will be the volume of ungasged fluidized bed, which is:

$$V_d = \sum_1^n V_{di} \quad (22)$$

The volume of ungasged fluidized bed is H_0A . The difference between V_d and H_0A is the dense phase in expanded area, of which the bed height is H' .

The bubble diameter D' can be obtained using equation (8).

Then the bubble volume of expanded area will be $n'V'_b$

The summation of each bubble phase will be:

$$V_b = \sum_1^n n_i V_{bi} + n'V'_b \quad (23)$$

Then the bed volume after expansion will be the summation of dense phase and bubble phase:

$$V_e = Aw + V_b, \quad (24)$$

$$H_e = \frac{V_e}{A}, \quad (25)$$

where w is the thickness of the fluidized bed, A is the cross-sectional area of the fluidized bed,

H_i is the initial bed height.

Therefore, the bed expansion e_3 will be calculated using equation (15).

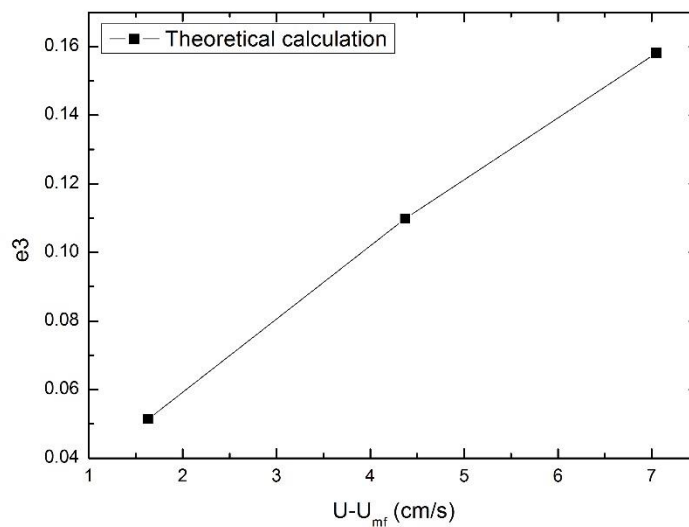


Figure 2.16 Bed expansion e_3 as a function of excess gas velocity ($U - U_{mf}$)

Figure 2.16 shows that bed expansion is proportional to the excess gas velocity. However, the results from theoretical calculation are independent of particle size and particle type.

2.3.6.3 Bed expansion by graphical analysis

A series of videos of fluidizing bed was recorded to analyze bubble characteristics. Each video

can be separated into consecutive frames using MATLAB. The number of bubbles (n) and bubble size (d_i) of each frame can be determined. Then the total volume of bubble phase can be calculated:

$$V_b = \frac{1}{4}\pi W \sum_{i=1}^n d_i^2 \quad (26)$$

The bed height after expansion will be:

$$H_e = H_0 + \frac{V_b}{A} \quad (27)$$

Then the bed expansion e_4 can be calculated using equation (15).

Figure 2.17 illustrates the bed expansion based on experimental videos. Every single point in Figure 2.17 represents the average bed expansion calculated from 10 frames. Magnetite (150-300 μm) and sand (150-300 μm) show the same pattern of bed expansion while sand (75-125 μm) and FCC catalyst (75-125 μm) behave in a different way. The bubbles of sand (75-125 μm) and FCC catalyst (75-125 μm) are too small to be captured by camera, which leads to errors on determination of bed expansion.

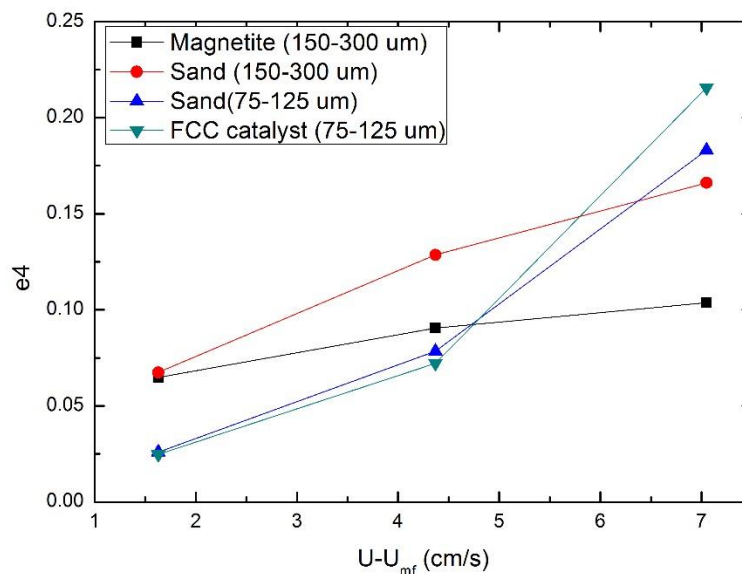


Figure 2.17 Bed expansion e_4 as a function of excess gas velocity $U-U_{mf}$

Table 2.3 Comparison between experimental bed expansion and theoretical bed expansion

Particles	U _g -U _{mf} (cm/s)	Experimental bed expansion		Theoretical calculation	
		e ₁	e ₂	e ₃	e ₄
Magnetite (150-300μm)	1.63	0.089	0.075	0.051	0.065
	4.37	0.145	0.085	0.110	0.090
	7.05	0.182	0.117	0.158	0.104
Sand (150-300μm)	1.63	0.032	0.059	0.051	0.067
	4.37	0.124	0.117	0.110	0.129
	7.05	0.184	0.152	0.158	0.166
Sand (75-125μm)	1.63	0.098	0.128	0.051	0.026
	4.37	0.158	0.160	0.110	0.078
	7.05	0.239	0.201	0.158	0.183
FCC catalyst (75-125μm)	1.63	0.134	0.126	0.051	0.025
	4.37	0.179	0.181	0.110	0.072
	7.05	0.257	0.215	0.158	0.216

Table 2.3 shows good agreement between experimental bed expansion and theoretical bed expansion of magnetite particles and sand (150-300 μm) particles while the discrepancy exists for FCC catalyst and sand (75-125 μm). Both FCC catalyst and sand (75-125 μm) belong to Geldart A type of particles, which have much smaller bubbles compared to Geldart B type of particles. However, these small bubbles cause some errors on bed expansion due to invisibility

under low superficial gas velocities.

2.3.7 Development of a new correlation for bubble diameter by the modification of Darton's equation

The correlation of bubble diameter proposed by Darton et al. in 1977 has been acknowledged extensively in the literature. Most experimental data Darton et al. used belonging to Geldart B type particles, including quartz sand, glass powder, alumina, and carbon to verify their correlation. Therefore the correlation of Darton cannot provide the best coverage for Geldart A type particles.

In addition, the theory developed by Darton et al. excluded mechanism of bubbles splitting and breakage. Therefore, a continuously increasing pattern of bubble diameter was obtained from their work. However, in real case, bubbles splitting and breakage do exist and are of critical importance for bubble size evolution. Horio and Wen (1977) pointed out that the equilibrium bubble size should be the result of a balance between bubble coalescence and break up.

It is discovered that bubble diameter D_e is sensitive to several parameters, including excess gas velocity $U_g - U_{mf}$, distance above the gas distributor "x", gas distributor hole diameter A_D and particle size d_p . In addition, the particle-fluid density ratio has not been found to affect the bubble diameter. Therefore, a functional relationship between these parameters and bubble diameter is proposed:

$$D_e = \phi(U - U_{mf})^\alpha (h + 4A_D^{0.5})^\beta \quad (28)$$

Where ϕ is a coefficient, related to particle size, h is the distance above gas distributor, A_D is

the diameter of holes on the distributor, α and β are constants.

In this work, two Geldart A type particles, one Geldart A/B type particles and one Geldart A type particles were utilized and a large number of experimental data of bubble diameter were obtained. Based on the large quantity of experimental data analyzed using curve fitting method in Matlab , a new modified correlation of bubble size is derived as:

$$D_e = \phi(U - U_{mf})^{0.204} (h + 4A_D^{0.5})^{0.759} / 1.2 \quad (29)$$

where

$$\phi = \begin{cases} 0.252 & \text{for Geldart B type of particles} \\ & \text{(magnetite and sand (150 - 300}\mu\text{m))} \\ 0.153 & \text{for Geldart A type of particles} \\ & \text{(magnetite and sand (150 - 300}\mu\text{m))} \end{cases}$$

Figure 2.18 shows calculated data against experimental results. Therefore, the proposed equation is in a good agreement with experimental data within 15% accuracy.

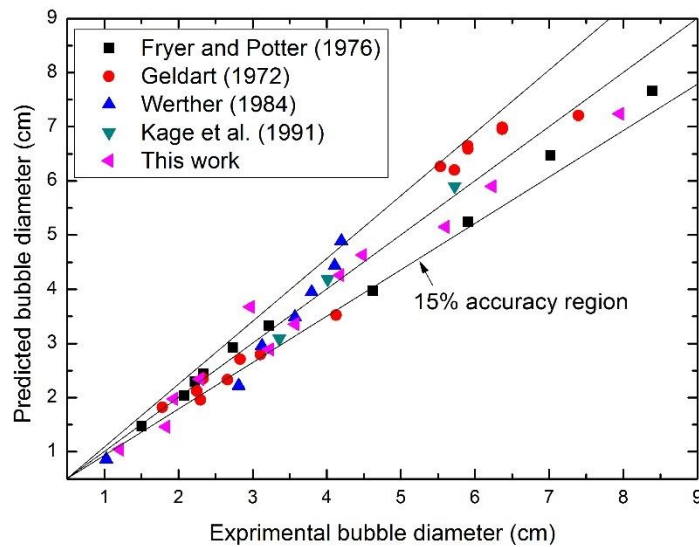


Figure 2.18 Comparison of experimental bubble diameter and predicted bubble diameter

2.3.8 Estimation of the bed density

The density of fluidized bed at a certain level is given by:

$$\bar{\rho}_{bed} = \rho_{bubble} \times \left(\frac{V_{bubble}}{V_{total}} \right) + \rho_{dense} \times \left(\frac{V_{dense}}{V_{total}} \right) \quad (30)$$

The gas volumetric flowrate in bubble phase (Davidson, 1985) is as follows:

$$G_b = (U_g - U_{mf})A \quad (31)$$

In the two-phase theory of fluidization, the bubble phase density is very close to the density of fluidizing gas, then the dense phase density can be taken as:

$$\rho_{dense} = \rho_p(1 - \varepsilon_{mf}) + \rho_g \varepsilon_{mf} \quad (32)$$

where,

$$\varepsilon_{mf} = \frac{H_{mf} - H_0}{H_0} \quad (33)$$

The gas bubble volume at a certain level is given by

$$V_b = A_b \times \Delta h = \frac{G_b \Delta h}{u_b} \quad (34)$$

The bubble rise velocity can be calculated using equation (9), which is:

$$u_b = 0.71\sqrt{gD_e} + (U_g - U_{mf}) \quad (9)$$

Then equation (34) will be

$$V_b = A_b \times \Delta h = \frac{G_b \Delta h}{u_b} = \frac{(U_g - U_{mf})A \Delta h}{0.71\sqrt{gD_e} + (U_g - U_{mf})} \quad (35)$$

In addition, the dense volume will be

$$V_d = A_d \Delta h = (A - A_b) \Delta h = \left(A - \frac{(U_g - U_{mf})A}{0.71\sqrt{gD_e} + (U_g - U_{mf})} \right) \Delta h \quad (36)$$

So, the density of fluidized bed (equation (30)) is as follows:

$$\begin{aligned}
\bar{\rho}_{bed} &= \rho_{bubble} \times \left(\frac{V_{bubble}}{V_{total}} \right) + \rho_{dense} \times \left(\frac{V_{dense}}{V_{total}} \right) = \rho_{bubble} \times \left(\frac{V_b}{A\Delta h} \right) + \rho_{dense} \times \left(\frac{V_d}{A\Delta h} \right) \\
&= \rho_b \left(\frac{(U_g - U_{mf})}{0.71\sqrt{gD_e} + (U_g - U_{mf})} \right) + \rho_d \left(1 - \frac{(U_g - U_{mf})}{0.71\sqrt{gD_e} + (U_g - U_{mf})} \right) \\
&= \rho_d + (\rho_b - \rho_d) \frac{(U_g - U_{mf})}{0.71\sqrt{gD_e} + (U_g - U_{mf})}
\end{aligned} \tag{37}$$

Combining equations (37) and (32);

$$\begin{aligned}
\bar{\rho}_{bed} &= \rho_d + (\rho_b - \rho_d) \frac{(U_g - U_{mf})}{0.71\sqrt{gD_e} + (U_g - U_{mf})} \\
&= \rho_p(1 - \varepsilon_{mf}) + \rho_g \varepsilon_{mf} + (\rho_g - \rho_p(1 - \varepsilon_{mf}) - \rho_g \varepsilon_{mf}) \frac{(U_g - U_{mf})}{0.71\sqrt{gD_e} + (U_g - U_{mf})} \\
&= (1 - \varepsilon_{mf})(\rho_p - \rho_g) \left(1 - \frac{(U_g - U_{mf})}{0.71\sqrt{gD_e} + (U_g - U_{mf})} \right) + \rho_g
\end{aligned} \tag{38}$$

where D_e can be calculated using equation (29), which is

$$D_e = \phi(U - U_{mf})^{0.204} (h + 4A_D^{0.5})^{0.0759} / 1.2 \tag{29}$$

where

$$\phi = \begin{cases} 0.252 & \text{for Geldart B type of particles} \\ & \text{(magnetite and sand (150 - 300}\mu\text{m))} \\ 0.153 & \text{for Geldart A type of particles} \\ & \text{(magnetite and sand (150 - 300}\mu\text{m))} \end{cases}$$

ε_{mf} can be calculated using equation (33), which is

$$\varepsilon_{mf} = \frac{H_{mf} - H_0}{H_0} \tag{33}$$

Therefore, the bed density of fluidized bed can be calculated using equation (38), (29) and

(33).

2.4 Conclusions

Bubble dynamics and bed expansion of four types of particles have been investigated in a 2D gas-solid fluidized bed using image processing technology. Based on the large quantity of analysis of experimental data, the relationships between bubble characteristics, bed expansion and particles, superficial gas velocity, the distance above gas distributor were obtained and

certain patterns could be observed:

- (i) Bubble size increases linearly with the distance above gas distributor, particles with a larger size tend to have a bigger bubble size for a given bed height.
- (ii) Bubbles of Geldart A type of particles can reach a maximum size due to more chance of break-up.
- (iii) Bubble rise velocity is proportional to the distance above gas distributor and larger bubbles rise faster than small bubbles.
- (iv) Geldart A type of particles have a bigger bed expansion than Geldart B type of particles due to huge amount of small bubbles in the bed.
- (v) A new correlation of bubble diameter is proposed and it shows a better prediction of bubble size compared to Darton's equation of bubble diameter.
- (vi) A method for estimation of bed density was developed based on the new correlation of bubble diameter.

Nomenclature

A_b, A	Surface area of a single bubble, cm^2
A_D	The diameter of hole on the distributor, m
d_p, d	Particle size, μm
D	Bubble diameter, m
D_e	Equivalent bubble diameter, cm
e	Bed expansion
F_d	Drag force, N
F_b	The buoyant force, N
g	Acceleration of gravity, m/s^2
H_0	Initial bed height, m
H_e	Expanded bed height, m
H, h	Bed height (The distance above gas distributor), m
Δt	Time interval between consecutive frames, s
u_b	Bubble rise velocity, cm/s
U_{mf}	The minimum fluidization velocity, cm/s
U	Superficial gas velocity, m/s
U	Velocity of fluid, m
V_b	Bubble volume, cm^3
w	Bed width, cm
x_i	Abscissa of bubble center, cm
y_i, y_{i-1}	Ordinate of bubble center, cm

ρ_p	The density of particles, kg/m ³
ρ_g	The density of fluidizing gas, kg/m ³
ρ_f	The density of fluidizing medium, kg/m ³
μ	Viscosity of fluidizing gas, Pa.s

Greek letters

ρ

μ

Reference

Andreux, R. and J. Chaouki (2005), Behaviors of the bubble, cloud, and emulsion phases in a fluidized bed, *AICHE Journal* 54: 406-414.

Busciglio, A., Vella, G., Micale, G. and L. Rizzuti (2010), Experimental analysis of bubble size distribution in 2D gas fluidized beds, *Chemical Engineering Science* 65: 4782-4791.

Coltters, R. and A.L. Rivas (2004), Minimum fluidization velocity correlations in particulate systems, *Powder Technology* 147 (1-3): 34-48.

Darton, R. C., LaNAUZE, R. D., Davidson, J. F. and D. Harrison (1977), Bubble growth due to coalescence in fluidized beds, *Trans. Inst. ChemE* 55: 274-280.

Davidson, J. F. and D. Harrison (1963), *Fluidized particles*, Cambridge university press.

Dwari, R. K. and K. H. Rao (2007), Dry beneficiation of coal-A review, *Mineral processing & extractive metallurgy review* 28 (3): 177-234.

Geldart, D. (1972), The size and frequency of bubbles in two and three dimensional gas fluidized beds, *Powder Technology* 4: 41-45.

Geldart, D. (1973), Types of gas fluidization, *Powder Technology* 7: 285-292.

Horio, M. and A. Nonaka (1987), A generalized bubble diameter correlation for gas-solid fluidized beds, *AICHE Journal* 33 (11): 1865-1872.

Halow, J. S., Fasching, G. E., Nicoletti, P. and J. L. Spenik (1993), Observation of a fluidized bed using capacitance imaging, *Chemical Engineering Science* 48: 643-659.

Lim, K. and P. Agarwal (1990), Conversion of pierced lengths measured at a probe to bubble size measures: an assessment of the geometrical probability approach and bubble shape models, *Powder Technology* 63: 205-219.

Lim, C., Glibertson, M. and A. Harrison (2007), Bubble distribution and behavior in bubbling fluidized beds, *Chemical Engineering Science* 62: 56-69.

McKeen, T. and T. Pugsley (2003), Simulation and experimental validation of a freely bubbling bed of FCC catalyst, *Powder Technology* 129: 139-152.

Ma, J., Liu, D. and X. Chen (2015), Bubble behaviors of large cohesive particles in a 2D fluidized bed, *Ind. Eng. Chem. Res.* 55: 624-634.

Mori, S. and C. Y. Wen (1975), Estimation of bubble diameter in gaseous fluidized beds, *AICHE*

Journal 21(1): 109-115.

Narsimhan, G. (1965), On a generalized expression for prediction of minimum fluidization velocity, *AIChE Journal* 11 (3): 550-554.

Park, W. H. and W. K. Kang (1969), The properties of bubbles in fluidized beds of conducting particles as measured by an electroresistivity probe, *Chemical Engineering Science* 24: 851-865.

Rowe, P. N. and B. A. Partridge (1965), An X-ray study of bubbles in fluidized beds, *Institution of Chemical Engineers* 43: 157-175.

Rowe, P.N. and C.X.R. Yacono (1976), The bubbling behaviour of fine powders when fluidized, *Chemical Engineering Science* 31: 1179-1192.

Sahu, A. K., Biswal, S. K. and A. Parida (2009), Development of air dense medium fluidized bed technology for dry beneficiation of coal – A review, *International Journal of Coal Preparation and Utilization* 29 (4): 216-241.

Van Houwelingen, J. A. and T. P. R. de Jong (2004), Automatic sorting and control in solid fuel processing: Opportunities in European perspective, *Geologica Belgica* 7 (3-4): 334-343.

Verma, V. and T.P. Johan (2014), Bubble dynamics in a 3-D gas–solid fluidized bed using ultrafast electron beam X-ray tomography and two-fluid model, *AIChE Journal* 60 (5): 1632-1644.

Werther, J. and O. Molerus (1973), The local structure of gas fluidized beds —I. A statistically based measuring system, *International Journal of Multiphase Flow* 1 (1): 103-122.

Whitehead, A.B., Dent, D.C. and G.N. Bhat (1967), Fluidization studies in large gas-solid systems-Part 1: bubble rise rates, *Powder Technology* 1: 143-148.

Werther, J. (1974), Influence of the bed diameter on the hydrodynamics of gas fluidized beds, *AIChE Symp. Ser.* 70 (141): 53-62.

Wen, C.Y. and Y.H. Yu (1966), A generalized method for predicting the minimum fluidization velocity, *AIChE Journal* 12 (3): 610-612.

Whitehead, A.B., Dent, D.C. and G.N. Bhat (1967), Fluidization studies in large gas-solid systems-Part 1: bubble rise rates, *Powder Technology* 1: 143-148.

Yasui, George and L. N. Johanson (1958), Characteristics of gas pockets in fluidized beds, *AIChE Journal* 4 (4): 445-452.

Chapter 3 Bubble dynamics and bed expansion in binary gas-solid fluidization

3.1 Introduction

Gas-solid fluidization technology, as an environmentally friendly alternative, has been widely applied in many industrial process, among which coal separation exhibits remarkable advantages over wet cleaning technology, such as no need for water, less air pollution, no slurry treatment and so on (Dwari, Rao 2007 and Houwelingen, Jong 2004). This specific gravity separation is achieved based on the difference of densities between medium solids and raw coal. In industrial process, density of fluidized bed can be adjusted by varying gas velocities. However, this adjustment controlled by gas velocity is not enough to meet the demand of low bed density. Therefore, binary mixture was introduced into the medium to substitute for single-component particles to lower down the bed density. In this way, a wider range of raw coal can be chosen to avoid energy-consuming pre-treatment processes.

The intense mixing between gas and particles enables gas-solid fluidization to yield higher mass and heat transfer rate between bubble phase and solid phase. The bubbles are generated when gas velocity exceeds the minimum fluidization velocity. In gas-solid fluidization, bubble behaviours have a significant effect on the fluidization quality, which ensures the efficiency of industrial processes (Lim, Gilbertson and Harrison 2007).

However, there are very few studies about bubble dynamics of mixtures of the particles in the past. The mixtures of particles can be divided into two categories: the same particles with different sizes and different particles with the same size. The first mixture is focusing on the effect of particle size on bubble dynamics, while the second is investigating the effect of particle density on bubble dynamics. Particles with larger size have the tendency to form bigger bubbles (Han et. al 2017), while the effect of particle density on bubble dynamics has not been

thoroughly studied.

There are limited studies on bubble dynamics as a function of fluidized bed properties in gas-solid fluidization in the literature. Furthermore, most of them are focusing on the bubble characteristics of single-component beds. Particle size effect seems to be of main concern in the study of bubble dynamics.

Various measurement systems have been developed to determine the bubble properties in fluidized beds, including different probes and photography. Several probe measurement systems, belonging to intrusive measurement technologies, have been utilized in recent years, which includes needle type capacitance probes (Werther, Molerus 1973), optical probes (Yasui and Johnson 1958, Andreux and Chaouki 2005) and electro-resistivity and conductivity probes (Park and Kang 1969). Photography technologies belonging to non-intrusive measurement technologies, are mainly composed of direct photography (Geldart 1970), X-ray photography (Rowe and Partridge 1965) and electrical capacitance tomography (Halow, Fasching, Nicoletti and Spenik 1993, McKeen and Pugsley 2003). In recent years, 2D fluidized bed has been widely utilized for the investigation of bubble dynamics in gas-solid fluidization due to its small thickness, which allows detail observation of bubbles in the fluidized bed.

Kage et al. (1991) performed the research of bubble sizes and bubble rising velocities in a gas-solid fluidized bed with mixtures of particles with different sizes but the same density using optic fiber probes. A new approach of determining bubble diameter in gas-solid fluidized bed with two-component particles was proposed. Muddle et al. (1994) investigated bubble behaviour of single-component particles in a 2D gas-solid fluidized bed using image

analysis technology. Special attention was paid to bubble properties and the results showed that determination of wake angle and wake area was possible. Busciglio et al. (2012) carried out a series of experiments to measure bubble characteristics in binary mixtures of corundum and glass particles with different sizes but the same density by means of digital imaging.

They did statistical analysis to describe bubble dynamics.

However, research studying the bubble dynamics of mixtures of particles with the same size but different densities as a function of fluidized bed properties is scarce. The main goal in this study is to measure bubble characteristics of binary mixtures of particles with the same size but different densities using image processing technology. In this work, bubble size, bubble rising velocity, bubble distribution and bed expansion were measured. Additionally, a correlation of determining bubble diameter in mixtures of particles with different densities was developed.

3.2 Experimental set-up and methods

3.2.1 Experimental set-up

Figure 3.1 shows the schematic diagram of the experimental setup. The fluidized bed designed for present study on bubble dynamics is made of Perspex (1500 mm height, 370 mm width and thickness of 19 mm), which provides detail observation of bubble behaviors inside the bed. There are three pressure measurement ports along the bed wall located at bed height of 0 mm, 180 mm and 550 mm. Two lights were placed in front of the fluidized bed to enhance the contrast between the bubble and dense phases, allowing more small bubbles being visualized. The bubble behaviors were recorded by a digital camera (Canon T3i), which was placed on the

opposite side of the bed. All videos were recorded at the steady state condition (complete fluidization).

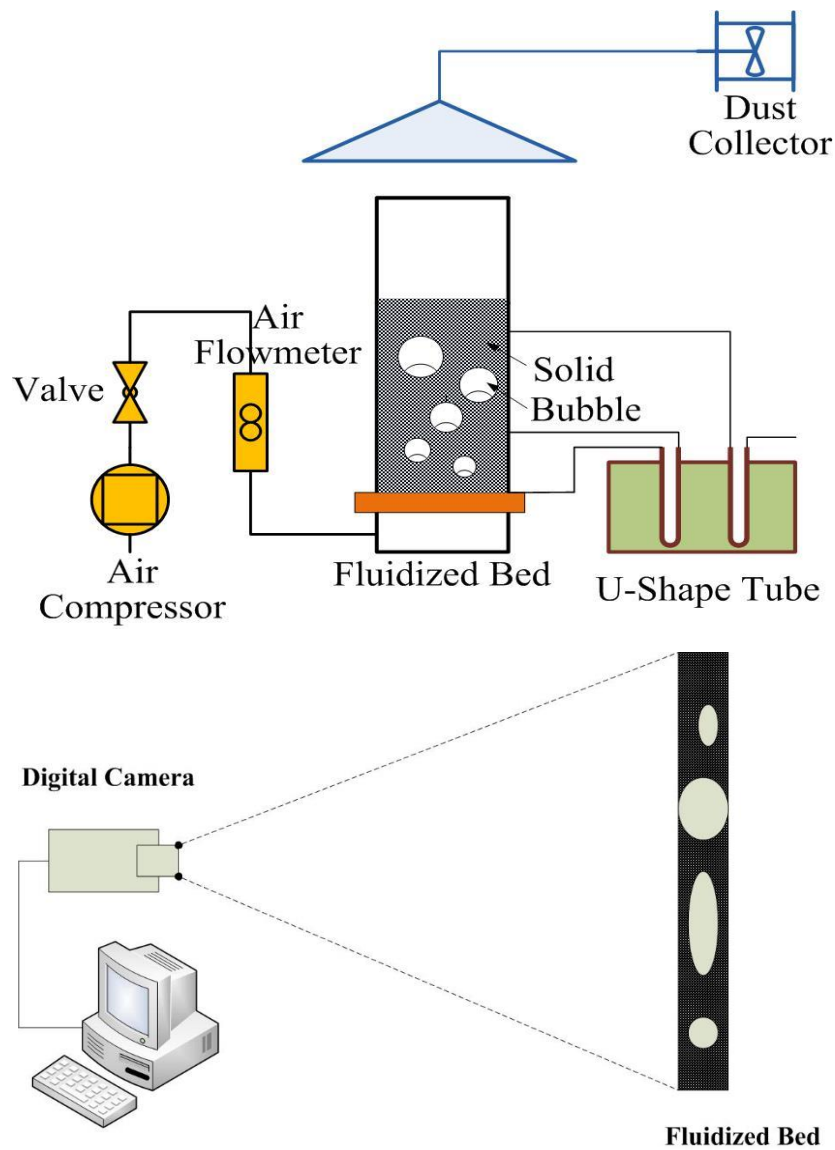


Figure 3.1 Schematic diagram of experimental equipment.

A sintered plastic gas distributor placed at the bottom of fluidized bed is designed with 10 micron holes. Below the gas distributor is the wind box used to ensure uniform distribution of inlet gas across the distributor. Air was used as the fluidizing gas and controlled by three air rotameters ranging from 0 m³/h to 5 m³/h.

Four binary mixtures composed of magnetite powder and sand with the same particle size

ranging from 150 μm to 300 μm and two single-component particles (magnetite powder, sand) were chosen. Binary mixtures having four compositions of 20%, 40%, 60% and 80% based on volume fraction of sand were used in the experiments. These 6 groups of experiments were studied at varying excess gas velocities of 7.05 cm/s, 4.37cm/s and 1.63cm/s with fixed bed height of 60 cm. Each binary mixture was fully mixed prior to the experiment. The properties of particles and binary mixtures are summarized in Table 3.1.

Table 3.1 Properties of particles and binary mixtures

Particle type	ρ_p (kg/m ³)	d_p (μm)	Geldart type
Magnetite powder	4650	150-300	B
Magnetite+Sand (20%)	4250	150-300	B
Magnetite+Sand (40%)	3850	150-300	B
Magnetite+Sand (60%)	3450	150-300	B
Magnetite+Sand (80%)	3050	150-300	B
Sand	2650	150-300	B

Table 3.1 shows that densities of binary mixtures are between density of magnetite powder and density of sand and they are decreasing with increasing volume fraction of sand.

3.2.2 Image processing

The bubble behaviors in the fluidized bed were videotaped after steady state condition was reached. The camera employed can record video at a frequency of 29 Hz, which implies 29

frames per second. Each frame is a 1088 X 1920 pixel picture. The pixel ranging from 0 to 255 is called grey-value which indicates brightness. Grey-value 0 is black while grey-value 255 means white. Each position in the picture has its own grey-value. In this way, pictures are transferred to a matrix, which can be analyzed using MATLAB (Matrix Laboratory).

The experimental procedure for image processing can be summarized into several steps : 1. Split the video into consecutive frames. 2. Transfer original RGB images into grey images. 3. Set a threshold to transfer grey images into binary images. 4. Do the subtraction of grey-value between fluidizing particles images and ungasged particles image to determine bubble properties. 5. Depict the contour of bubbles and obtain bubble characteristics applying a package of software 'Regionprops'. A video used as the base was recorded before air was introduced into the bed. Then grey-value's difference between the base image and images of the fluidized bed of every position was obtained. A non-zero grey-value difference implies a position where bubble exists due to different grey-values between the dense and bubble phases.

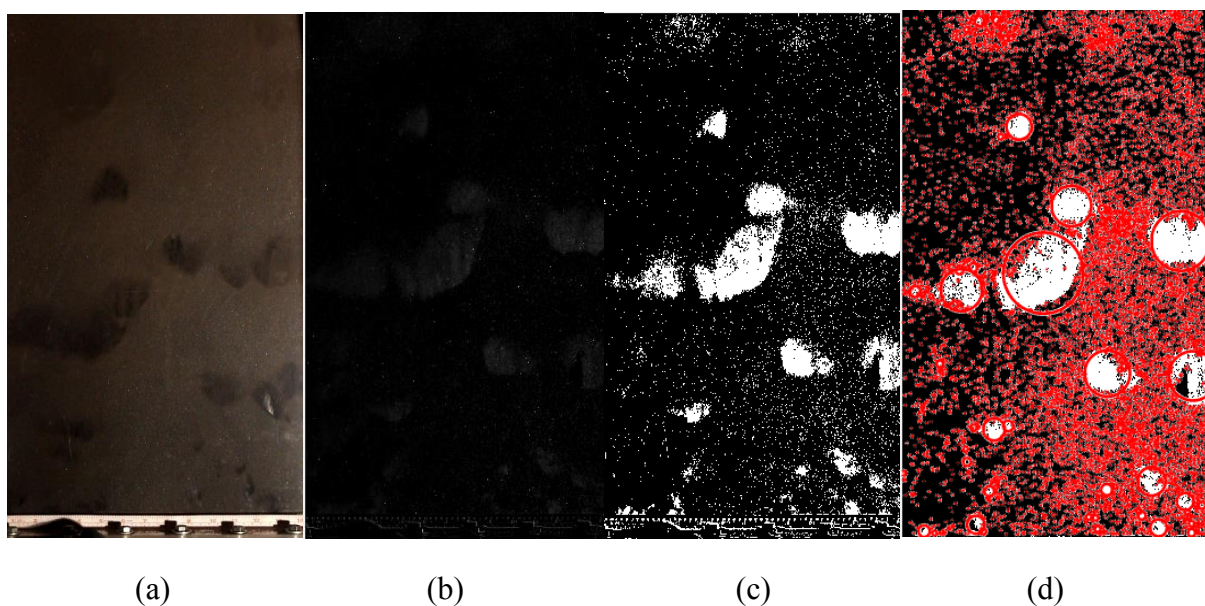


Figure 3.2 Image processing procedure: (a) Original RGB image (b) Grey image (c) Binary

image (d) Image with circles.

3.2.3 Bubble size

The bubble phase was discriminated from the dense phase based on the grey-value difference. However, a threshold needs to be determined to improve the discrimination between these two phases because of the distraction of noise points. In this study, the threshold was determined to be 10 to exclude noise points. The area of a bubble (A_b) is the number of pixels forming this bubble. Every single bubble was transmitted to a circle with the same area using a software called Regionprops. According to the bubble area, the equivalent bubble diameter D_e can be calculated from the following equation:

$$D_e = 2 \sqrt{\frac{A_b}{\pi}} \quad (1)$$

3.2.4 Bubble rising velocity

The camera applied in this investigation recorded videos of 29 frames per second. Therefore, the time interval (Δt) between every two consecutive frames is 1/29 second. The coordinates (x_i, y_i) of bubble center in each frame can be determined automatically by means of the image processing technology. In this way, the axial distance ($y_i - y_{i-1}$) that every single bubble moves between every two consecutive frames was obtained. Then the bubble rising velocity can be calculated from the following equation:

$$u_b = \frac{y_i - y_{i-1}}{\Delta t} \quad (2)$$

3.3 Results

3.3.1 The minimum fluidization velocity (U_{mf})

The minimum fluidization velocity is the fluid velocity at incipient fluidization of a packed bed filled up with particles. It is a critical variable for designing fluidized beds. In this study, the minimum fluidization velocity (U_{mf}) is determined by measuring the pressure drop as a function of superficial gas velocity (shown in Figure 2.3).

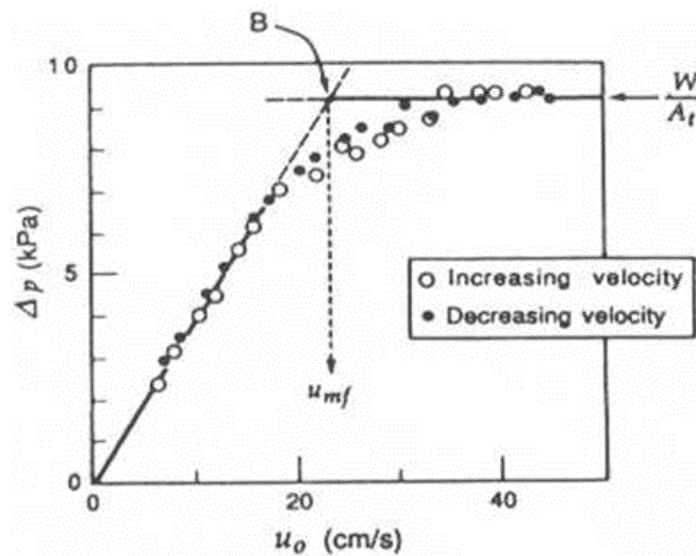


Figure 3.3 Pressure drop against superficial gas velocity

Pressure drop remains nearly constant after superficial gas velocity exceeds certain limit. This limit is determined as the minimum fluidization velocity, at which particles inside the bed begin to fluidize. Figure 3.4 shows that the minimum fluidization velocity of the binary mixtures decreases with increasing volume fraction of lighter (sand) particles. It reveals that the minimum fluidization velocity of heavy particles can be reduced by addition of lighter particles, which means sand particles are easier to be fluidized than magnetite powder. The fluidizing gas can support the weight of whole bed of particles when it reaches the minimum fluidization velocity. Therefore superficial gas velocity which makes particles completely fluidized is also decreasing with increasing volume fraction of the sand particles.

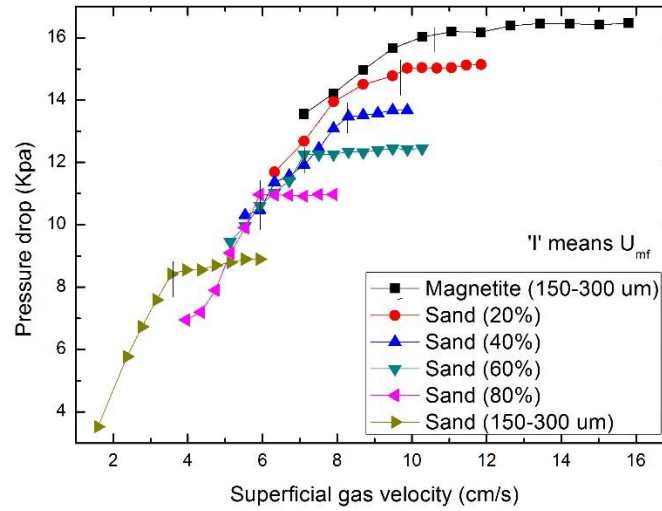


Figure 3.4 The minimum fluidization velocities of binary mixtures.

Many correlations for predicting minimum fluidization velocity have been developed, such as correlations of Narsimhan (1965), Wen and Yu (1966) and Coltters and Rivas (2004).

According to these correlations, the minimum fluidization velocity has a main dependency of particles and gas properties, such as densities, particles sphericity and diameter, and voidage at U_{mf} (Coltters and Rivas 2004).

Noda et al. (1986) proposed a new correlation for the prediction of the minimum fluidization velocity for binary mixtures by the modification of the equation of Wen and Yu (1966). The equation of Wen and Yu for the minimum fluidization velocity for single-component systems is described as follows:

$$A_r = 24.5Re_{mf}^2 + 1650Re_{mf} \quad (3)$$

where

$$A_r = d^3 \rho_g (\rho_f - \rho_g) \frac{g}{\mu^2} \quad (4)$$

$$Re_{mf} = \frac{d \rho_g \mu_{mf}}{\mu} \quad (5)$$

The diameter and density of binary mixtures in this work need to be modified to apply

equation (3).

$$\bar{\rho} = \rho_m V_m + \rho_s V_s \quad (6)$$

$$\bar{d} = \sqrt[3]{(d_m^3 + d_s^3)} \quad (7)$$

Then the equation can be rewritten as

$$A_r = A Re_{mf}^2 + B Re_{mf} \quad (8)$$

where A and B are constants.

Noda et al. determined these two parameters, which are given by

$$A = 36.2 \left(\frac{d_m \rho_f}{\bar{d} \rho_m} \right)^{-0.196} \quad (9)$$

$$B = 1397 \left(\frac{d_m \rho_f}{\bar{d} \rho_m} \right)^{0.296} \quad (10)$$

A comparison between U_{mf} of these correlations and experimental U_{mf} is shown in Table 3.2.

Table 3.2 Comparison for minimum fluidization velocity

Particles	P(kg/m ³)	U_{mf} predicted (cm/s)		
		Wen/Yu	Noda et al.	This work Experiment
Magnetite+Sand (20%)	4250	7.01	8.23	9.51
Magnetite+Sand (20%)	3850	6.36	7.69	8.37
Magnetite+Sand (20%)	3450	5.70	7.12	7.24
Magnetite+Sand (20%)	3050	5.04	6.53	5.93

Table 3.2 shows that modified correlation proposed by Noda et al. for binary systems fits experimental data better than the equation of Wen and Yu, which implies hydrodynamics of binary fluidization are different from that of single-component systems.

3.3.2 Bubble size evolution

When particles in the fluidized bed are fluidized by an upward flow of gas, bubbles are formed by excess gas flow based on the superficial gas velocity exceeding the minimum fluidization velocity. Bubbles formed at the bottom rise through the bed to the surface.

During this process, bubbles continually coalesce and break up reaching a balance of varying bubble diameters (Horio and Nonaka 1987).

Mori and Wen (1975) proposed a correlation of bubble diameter and growth in fluidized beds based on initial bubble diameter and maximum bubble diameter. Furthermore, the bubble diameters calculated from this correlation are in good agreement with the bubble sizes observed.

The proposed correlation for predicting bubble diameters of Mori and Wen is given by;

$$\frac{D_{BM}-D_B}{D_{BM}-D_{B0}} = \exp(-0.3 h/D_t) \quad (11)$$

where

$$D_{B0} = 0.00376(U - U_{mf})^2 \quad (12)$$

For the porous plate distributor

$$D_{BM} = 0.652\{A_t(U - U_{mf})\}^{0.4} \quad (13)$$

Where D_B is the bubble diameter, D_{BM} is the maximum bubble diameter, D_{B0} is the initial bubble diameter, D_t is the bed diameter, A_t is the cross-sectional area of the bed, and h is the distance above gas distributor.

Darton's equation (Darton et al. 1977) for bubble diameter is the most widely used by researchers due to its good coverage under all conditions. However, this correlation excluded mechanism of bubbles splitting and breakage. Therefore, a continuously increasing pattern of bubble diameter was obtained from their work (Karimipour and Pugsley 2011). However, in

real cases, bubbles splitting and breakage do exist and are of critical importance for bubble size evolution. The equation of Darton et al. is as follows:

$$D_e = 0.54g^{-0.2}(U - U_{mf})^{0.4}(h + 4A_D^{0.5})^{0.8} \quad (14)$$

A new correlation for the estimation of bubble diameter was proposed in this work by the modification of the equation of Darton and it is given by

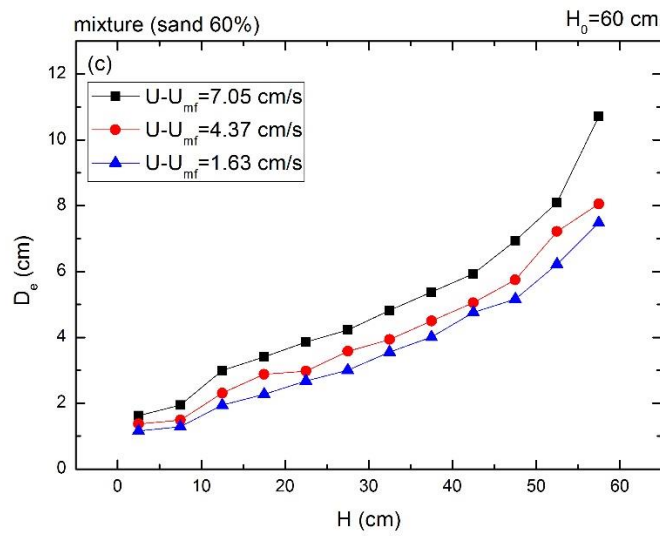
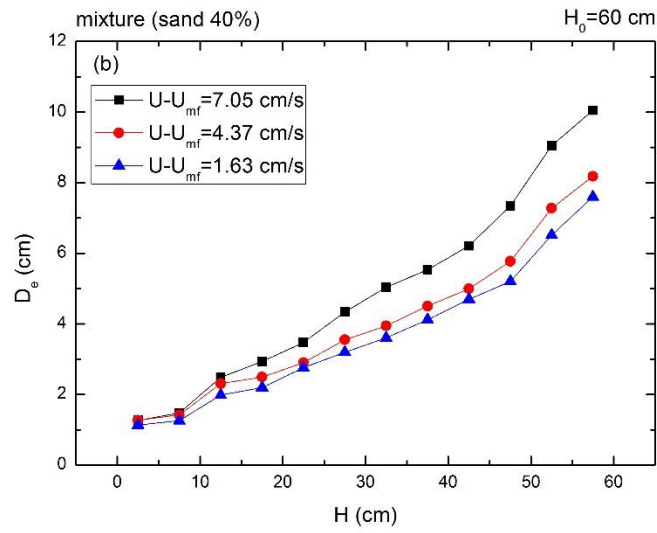
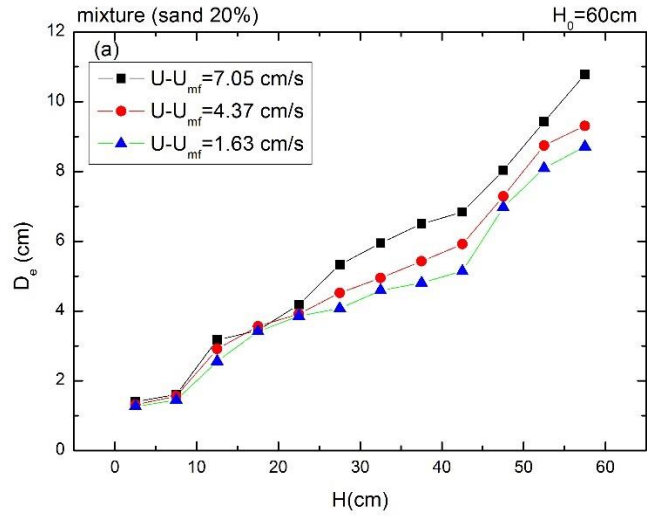
$$D_e = \phi(U - U_{mf})^{0.204}(h + 4A_D^{0.5})^{0.759/1.2} \quad (15)$$

where

$$\phi = \begin{cases} 0.252 & \text{for Geldart B type of particles} \\ & \text{(magnetite and sand (150 - 300}\mu\text{m))} \\ 0.153 & \text{for Geldart A type of particles} \\ & \text{(magnetite and sand (150 - 300}\mu\text{m))} \end{cases}$$

where U is the superficial gas velocity, U_{mf} is the minimum fluidization velocity, A_D is the diameter of the hole on the gas distributor.

Figure 3.5 illustrates that bubble diameter is increasing with the distance above gas distributor. In addition, bubble diameter is also proportional to excess gas velocity. Bubbles of binary mixtures have similar growth patterns with bubbles of single-component particles as a function of excess gas velocity and bed height. Bubbles coalesce as they rise through the bed and grow larger. Another reason for larger bubbles at higher level is due to the lower hydrostatic pressure at higher elevations. Coalescence dominates the growth compared to decreasing bed hydrostatic pressure. More gas is introduced into the bed when the gas velocity is higher, which means more chance for coalescence to form big bubbles.



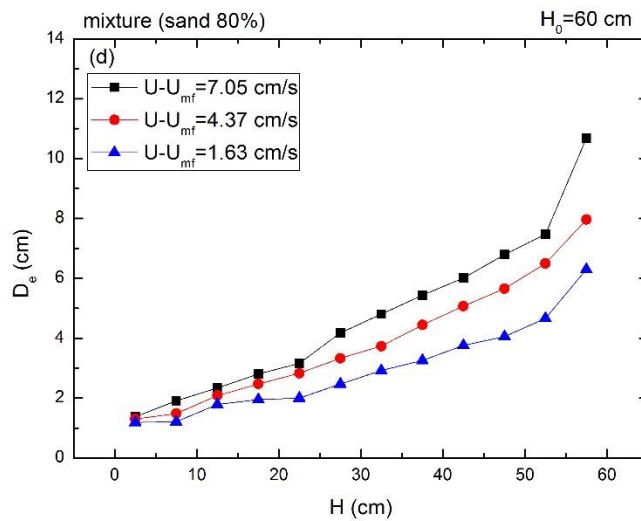
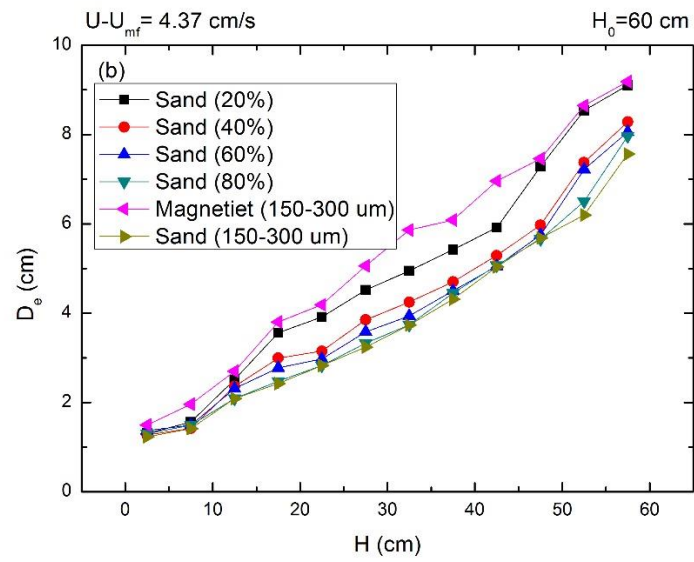
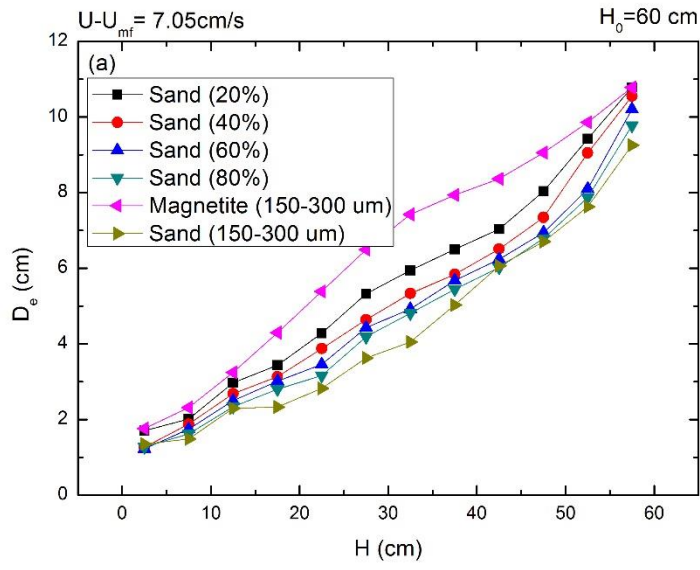


Figure 3.5 Bubble size of binary mixtures as a function of the distance above gas distributor.

Figure 3.6 shows the comparison of bubble diameter between two single-component particles and four binary mixtures. It is clear that bubble diameters of binary mixtures are reduced by the addition of light (sand) particles. Magnetite powder has larger bubbles while sand particles have smaller bubble diameter. The bubble diameters of four binary mixtures fall in between magnetite powder and sand particles and bubble sizes are decreasing with increasing volume fraction of sand particles. According to the results found in bubble sizes of single-component particles, light sand particles have smaller bubbles than heavy magnetite powder. Therefore, bubble size can be reduced when light sand particles are added. The fluidizing gas has to overcome the gravity of particles by upward drag force exerted on particles. For heavy particles, it is harder to be fluidized so that gas tends to accumulate in the gas phase and form larger bubbles.



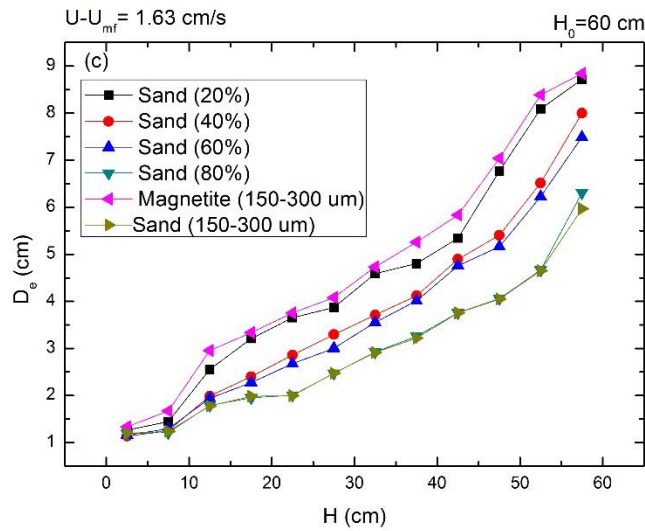


Figure 3.6 Bubble size of single-component particles and binary mixtures.

Figure 3.7 (a) describes the bubble size distribution of single-component particles of magnetite and Figure 3.7 (b) illustrates the bubble size distribution of binary mixture with 20% (vol.%) of sand. It is clear that small bubbles population grows larger by the addition of light sand particles and these small bubbles homogeneously spread out throughout the bed. Therefore, the addition of light sand particles gives magnetite powder a better fluidization quality. In addition, according to Figure 3.6, the average bubble sizes of binary mixtures are reduced due to the increased ratio between small bubbles and large bubbles.

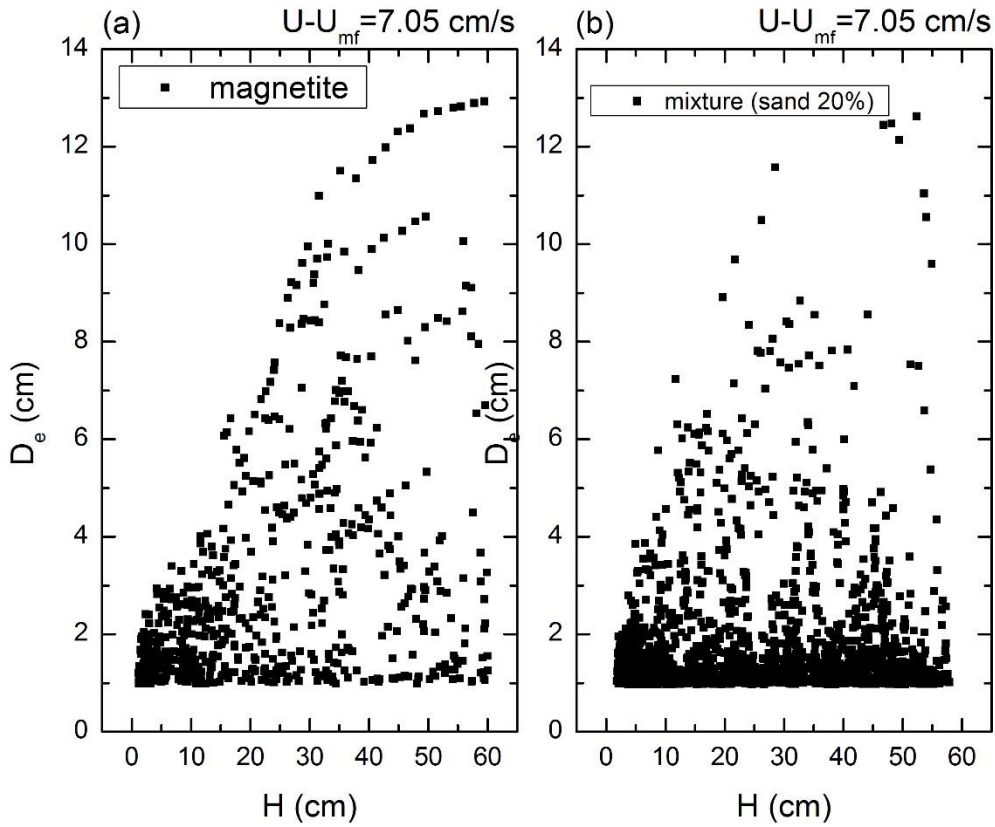


Figure 3.7 Bubble distribution of magnetite and binary mixture (sand 20%).

A new correlation for estimation of bubble diameter was proposed by Han et al. by the modification of Darton's equation, which is shown as equation (15).

$$D_e = \phi(U - U_{mf})^{0.204} (h + 4A_D^{0.5})^{0.759} / 1.2 \quad (15)$$

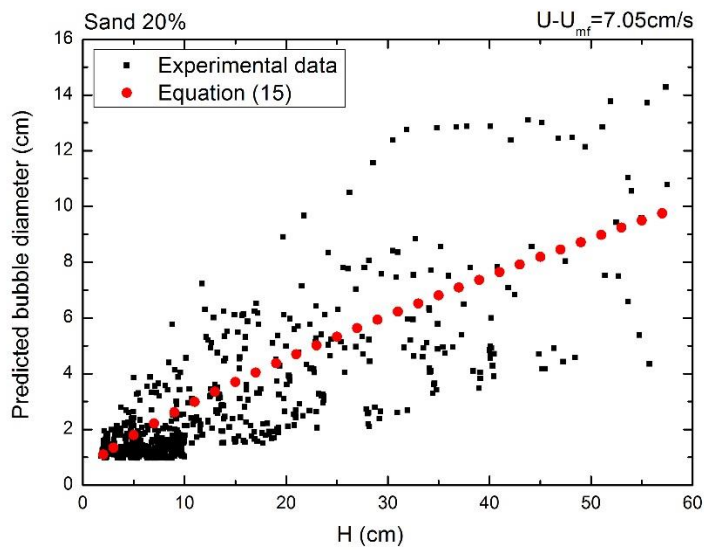
where

$$\phi = \begin{cases} 0.252 & \text{for Geldart B type of particles} \\ & \text{(magnetite and sand (150 - 300}\mu\text{m))} \\ 0.153 & \text{for Geldart A type of particles} \\ & \text{(magnetite and sand (150 - 300}\mu\text{m))} \end{cases}$$

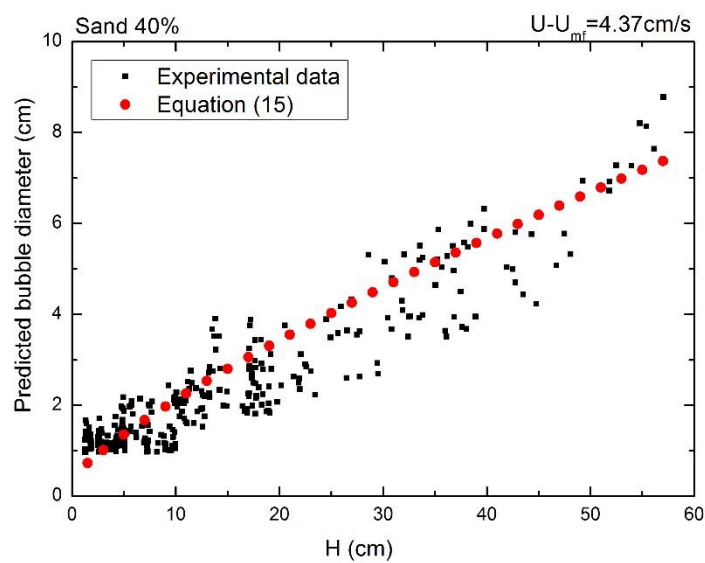
Figure 3.8 shows a comparison between bubble diameters calculated from equation (10) and the experimental values. The red points, standing for calculated bubble sizes using equation (10), are increasing with bed height and lie in the center region of experimental values.

Therefore they are in good agreement with the average bubble diameters. So, the correlation for estimation of bubble diameter for single-component particles also gives a good prediction of bubble size of the binary mixtures, which means equation (10) can be suitable for both single-component and binary systems.

(a)



(b)



(c)

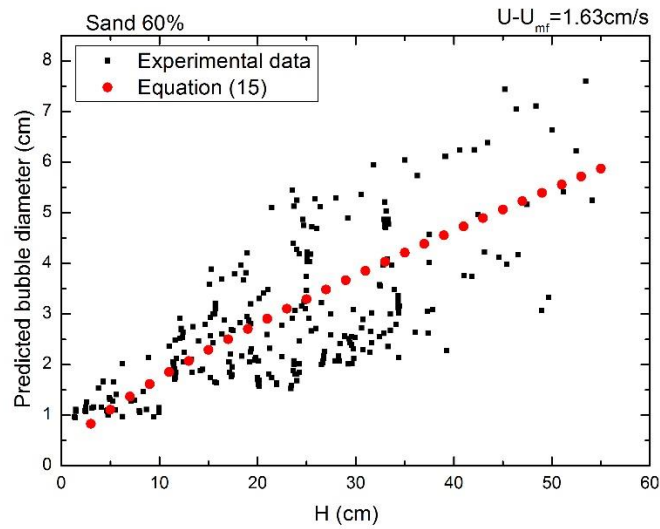


Figure 3.8 Bubble diameters calculated from equation (10) compared with experimental data.

3.3.3 Bubble rise velocity

Davison and Harrison (1963) developed the most widely used equation for bubble velocity.

The correlation for bubble rise velocity is given by

$$u_b = 0.71\sqrt{gD_e} + (U - U_{mf}) \quad (16)$$

Where D_e is the bubble diameter, U is superficial velocity and U_{mf} is the minimum fluidization velocity.

Corresponding to this correlation, bubble rising velocity is dominated by the bubble diameter and the excess gas velocity.

Werther (1978) investigated the bubble rise velocities of FCC catalyst and sand particles using a capacitance probe. A correlation for prediction of bubble rise velocity of Geldart A and B type of particles was proposed as follows:

$$u_b = k\sqrt{gD_e} \quad (17)$$

For Geldart A type of particles:

$$k = \begin{cases} 1 & d_p \leq 10 \\ 0.396d_p^{0.4} & 10 < d_p < 100 \\ 2.5 & d_p \geq 100 \end{cases} \quad (18)$$

For Geldart B type of particles:

$$k = \begin{cases} 0.64 & d_p \leq 10 \\ 0.254d_p^{0.4} & 10 < d_p < 100 \\ 1.6 & d_p \geq 100 \end{cases} \quad (19)$$

Where d_p is the particle size.

According to Werther's equation, bubble rise velocity is depended on the bubble size and particle size.

Figure 3.9 shows that bubble rise velocity is increasing with increasing distance above the gas distributor and proportional to excess gas velocity. Bubble rise velocity has the same growth pattern with that of single-component particles in terms of bed height and excess gas velocity.

According to the equation of Davidson and Harrison and the equation of Werther, bubble rise velocity is dominated by the bubble size. Bubble rise velocity is increasing with increasing bubble size due to forces exerted on the bubbles. Specific analysis of forces acted on the bubbles is provided elsewhere (see Chapter 1).

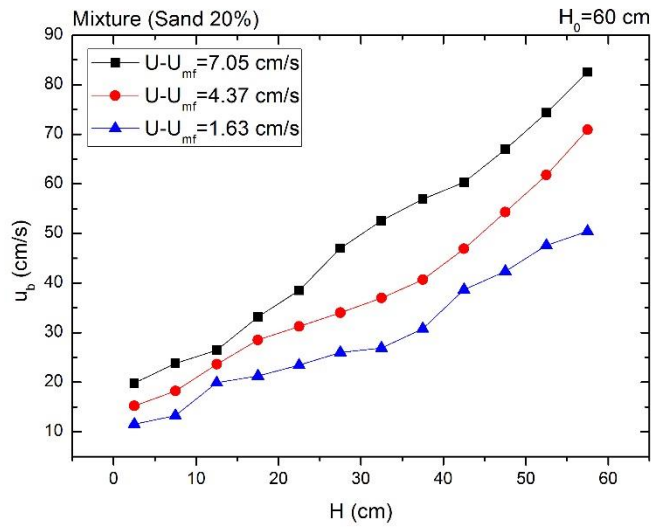


Figure 3.9 Bubble rise velocity as a function of the distance above gas distributor.

Figure 3.10 illustrates the bubble rise velocities of four binary mixtures and two single-component particles. The bubble rise velocities of four binary mixtures are in between bubble rise velocity of magnetite powder and sand particles and the bubble rise velocities are decreasing with increasing volume fraction of sand particles. Magnetite powder still has the biggest bubble rise velocities, while sand particle has the minimum bubble rise velocity. The growth pattern of bubble rise velocity completely matches that of bubble size and the match between bubble rise velocity and bubble size verifies that bubble rise velocity is dominated by bubble size.

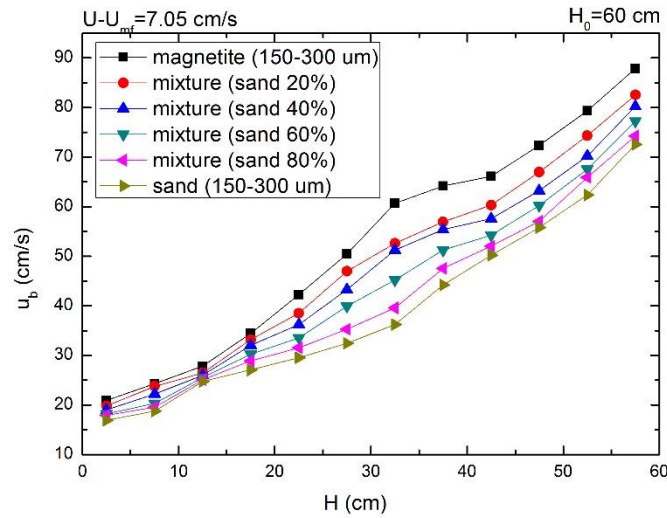


Figure 3.10 A comparison of bubble rise velocities between mixtures and single-component particles.

3.3.4 Bed expansion

3.3.4.1 Experimental

The bed surface is forced up to a higher level when particles inside the bed are fluidized due to additional volume occupied by bubbles. Therefore, bed expansion is of critical importance to determine the amount of solid and gas bubbles. In this work, two methods were applied to measure the bed expansion. One method is direct observation of the expanded bed height while the other is through the pressure drop measurement. Ten pictures were taken during the first method to obtain average expanded bed height (H_e) with known initial bed height (H_0). Then the bed expansion (e_1) can be calculated based on the following formula:

$$e = \frac{H_e - H_0}{H_0} \quad (20)$$

The average density of the whole bed is obtained by pressure drops along the bed. The relationship between pressure drop and expanded bed height can be described as follows:

$$\Delta p = \rho g h \quad (21)$$

Then expanded bed height H_e can be calculated and bed expansion (e_2) will be obtained using equation (20).

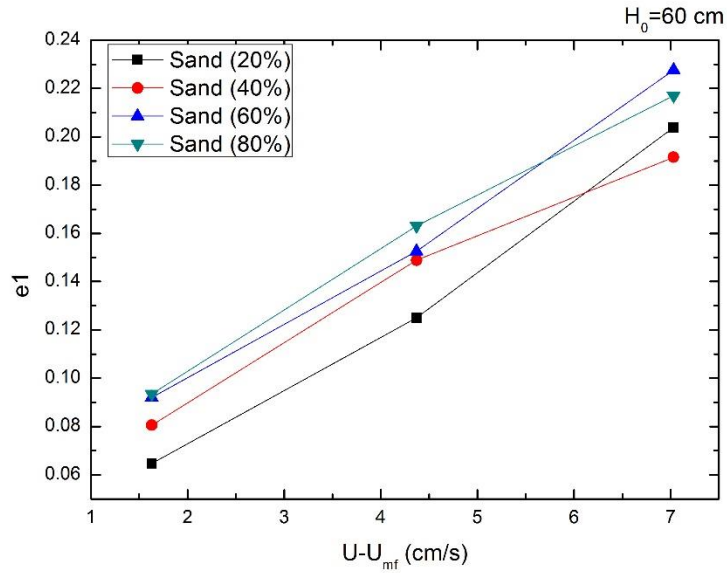


Figure 3.11 Bed expansion e_1 as a function of excess gas velocity

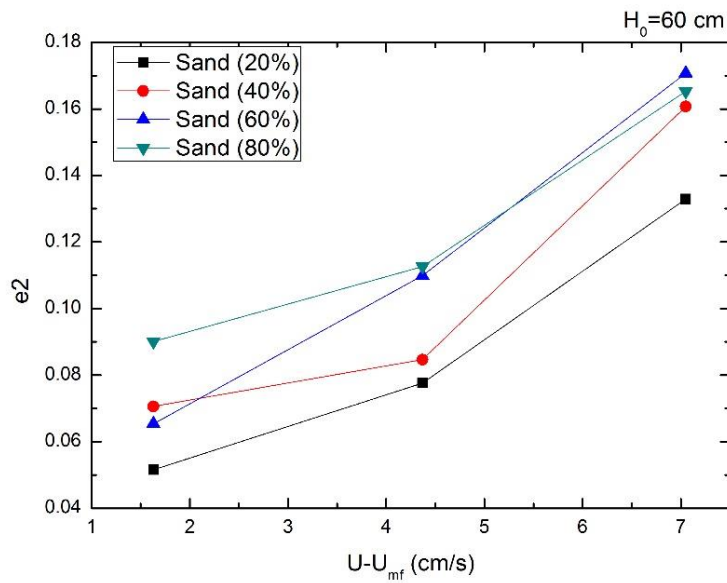


Figure 3.12 Bed expansion e_2 as a function of excess gas velocity.

Figure 3.11 and Figure 3.12 show the be expansion data obtained through these two methods.

It is observed that bed expansion is proportional to excess gas velocity. The reason is that higher excess gas velocity means more gas bubbles rising through the bed. Then the space occupied by gas bubbles increases resulting in a bigger bed expansion. In addition, binary mixtures with bigger volume fraction of lighter (sand) particles tend to have bigger bed expansions, which is because of the fact that sand particles have larger small bubbles population contributing to larger volume of bubble phase compared to magnetite powder. These patterns are more obvious in the bed expansion data of the second method. The experimental bed expansion data obtained from the direct observation might have some errors due to intense fluctuation of bed surface during the measurements.

3.3.4.2 Theoretical

Bubbles grow bigger and move faster when they rise through the fluidized bed. Therefore, there are specific bubble size and bubble rise velocity at each position. An iteration method was used to obtain expanded bed height. The fluidized bed was divided into equally spaced sections with a height of H_i . Each section has its own serial number “n” as a marker. Bubble diameter d_i and bubble velocity v_i in each part can be calculated using bubble size equation (15) and bubble velocity equation (16).

Based on mass balance on the gas phase, the number of bubbles in each part can be obtained using following equations:

$$D_e = \phi(U - U_{mf})^{0.204} \left(\frac{H_i}{2} + (n - 1)H_i + 4A_D^{0.5} \right)^{0.759} / 1.2 \quad (22)$$

where

$$\phi = \begin{cases} 0.252 & \text{for Geldart B type of particles} \\ & \text{(magnetite and sand (150 – 300}\mu\text{m))} \\ 0.153 & \text{for Geldart A type of particles} \\ & \text{(magnetite and sand (150 – 300}\mu\text{m))} \end{cases}$$

A single bubble volume will be:

$$V_{bi} = \frac{1}{4}\pi D_i^2 w \quad (23)$$

where w is the thickness of the fluidized bed.

Then the bubble rising velocity will be:

$$u_{bi} = 0.71\sqrt{gD_i} + U - U_{mf} \quad (24)$$

The time bubble stays in each part will be:

$$t = \frac{H_i}{u_{bi}} \quad (25)$$

Then the number of bubbles in each part will be:

$$n_i = \frac{(U_g - U_{mf})t}{V_b} \quad (26)$$

Then the dense phase volume will be:

$$V_{di} = AH_i - n_i V_{bi} \quad (27)$$

where A is cross-sectional area of the fluidized bed

The summation of each dense phase volume will be the volume of ungasged fluidized bed, which is:

$$V_d = \sum_1^n V_{di} \quad (28)$$

The volume of ungasged fluidized bed is H_0A . The difference between V_d and H_0A is the dense phase in expanded area, of which the bed height is H' .

The bubble diameter D' can be obtained using equation (15).

Then the bubble volume of expanded area will be $n'V'_b$

The summation of each bubble phase will be:

$$V_b = \sum_1^n n_i V_{bi} + n' V'_b \quad (29)$$

Then the bed volume after expansion will be the summation of dense phase and bubble phase:

$$V_e = Aw + V_b, \quad (30)$$

$$H_e = \frac{V_e}{A}, \quad (31)$$

Therefore, the bed expansion e_3 will be calculated using equation (20).

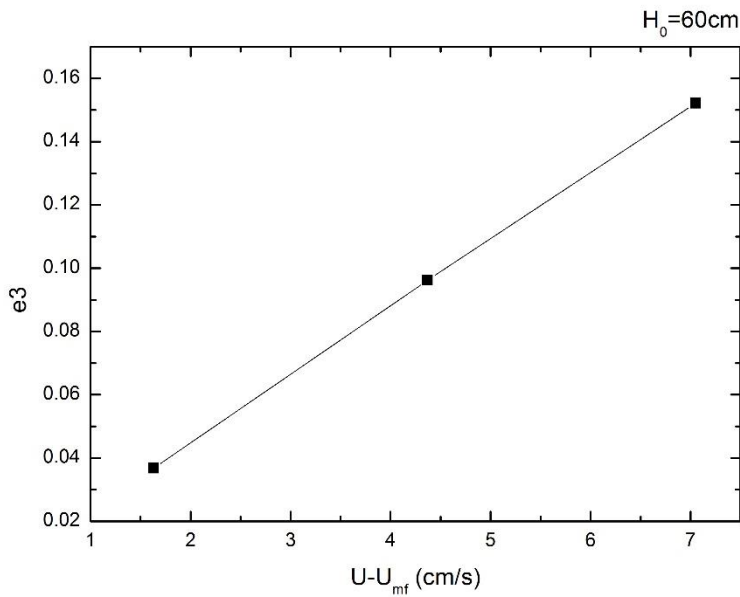


Figure 3.13 Bed expansion e_3 as a function of excess gas velocity

Figure 3.13 shows that bed expansion increases linearly with increasing excess gas velocity.

However, the calculation of bed expansion is completely depend on the distance above the gas distributor, which means it cannot reflect the relationship between bed expansions of different particles.

In addition, the frames of fluidizing particles recorded can clearly give us the number of bubbles n and bubble size D_i of each bubble. Each single bubble volume can be calculated from the equation (23). Then the total volume of bubble phase will be:

$$V_b = \sum_1^n V_{bi} \quad (32)$$

Then the bed expansion e_4 can be obtained from equations (30), (31) and (20).

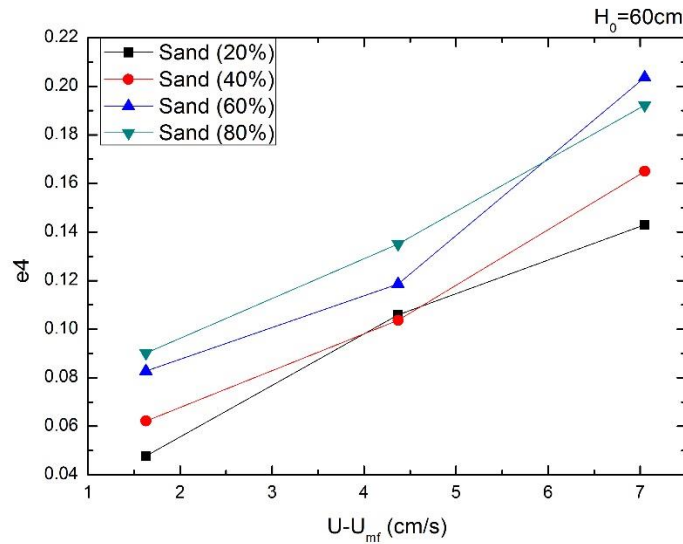


Figure 3.14 Bed expansion e_4 as a function of excess gas velocity

Figure 3.14 illustrates that the bed expansion obtained from fumes showed bigger bed expansions at 0.6 and 0.8 volume fraction of sand particles while bed expansions at 0.6 volume fraction did show a bigger value at lowest excess gas velocity. It is the undetected small bubbles population that led to this discrepancy. Small bubbles of which bubble sizes are lower than 1.9 cm have a high possibility of not being recorded due to the limited thickness of the bed.

Table 3.3 Comparison between experimental bed expansion and theoretical bed expansion

Particles	$U_g - U_{mf}$ (cm/s)	Experimental bed expansion		Theoretical calculation	
		e_1	e_2	e_3	e_4
Mixture(sand 20%) (150-300 μm)	1.63 4.37 7.05	0.065 0.125 0.204	0.052 0.078 0.133	0.051 0.110 0.158	0.048 0.106 0.143
Mixture(sand 40%) (150-300 μm)	1.63 4.37 7.05	0.081 0.149 0.192	0.071 0.085 0.161	0.051 0.110 0.158	0.082 0.104 0.165
Mixture(sand 60%) (150-300 μm)	1.63 4.37 7.05	0.092 0.153 0.228	0.065 0.110 0.171	0.051 0.110 0.158	0.083 0.119 0.204
Mixture(sand 80%) (150-300 μm)	1.63 4.37 7.05	0.093 0.163 0.217	0.090 0.113 0.165	0.051 0.110 0.158	0.090 0.135 0.192

Table 3.3 shows a good agreement between the experimental bed expansion and theoretical bed expansion data. The bed expansion value obtained through the first method tends to have a bigger value due to the errors caused by the intense fluctuation of the bed surface.

3.3.5 Bed density estimation of binary gas-solid fluidization systems

The density of fluidized bed at a certain level is given by

$$\bar{\rho}_{bed} = \rho_{bubble} \times \left(\frac{V_{bubble}}{V_{total}} \right) + \rho_{dense} \times \left(\frac{V_{dense}}{V_{total}} \right) \quad (33)$$

The gas volumetric flowrate in bubble phase (Davidson, 1985) is as follows:

$$G_b = (U_g - U_{mf})A \quad (34)$$

In the two-phase theory of fluidization, the bubble phase density is very close to the density of fluidizing gas, then the dense phase density can be taken as:

$$\rho_{dense} = \rho_p(1 - \varepsilon_{mf}) + \rho_g \varepsilon_{mf} \quad (35)$$

where

$$\varepsilon_{mf} = \frac{H_{mf} - H_0}{H_0} \quad (36)$$

The gas bubble volume at a certain level is given by

$$V_b = A_b \times \Delta h = \frac{G_b \Delta h}{u_b} \quad (37)$$

The bubble rise velocity can be calculated using equation (9), which is:

$$u_b = 0.71\sqrt{gD_e} + (U_g - U_{mf}) \quad (9)$$

Then the equation (34) will be:

$$V_b = A_b \times \Delta h = \frac{G_b \Delta h}{u_b} = \frac{(U_g - U_{mf})A \Delta h}{0.71\sqrt{gD_e} + (U_g - U_{mf})} \quad (38)$$

In addition, the dense volume will be:

$$V_d = A_d \Delta h = (A - A_b) \Delta h = \left(A - \frac{(U_g - U_{mf})A}{0.71\sqrt{gD_e} + (U_g - U_{mf})} \right) \Delta h \quad (39)$$

So, the density of fluidized bed (equation (33)) is as follows:

$$\begin{aligned} \bar{\rho}_{bed} &= \rho_{bubble} \times \left(\frac{V_{bubble}}{V_{total}} \right) + \rho_{dense} \times \left(\frac{V_{dense}}{V_{total}} \right) = \rho_{bubble} \times \left(\frac{V_b}{A \Delta h} \right) + \rho_{dense} \times \left(\frac{V_d}{A \Delta h} \right) \\ &= \rho_b \left(\frac{(U_g - U_{mf})}{0.71\sqrt{gD_e} + (U_g - U_{mf})} \right) + \rho_d \left(1 - \frac{(U_g - U_{mf})}{0.71\sqrt{gD_e} + (U_g - U_{mf})} \right) \end{aligned}$$

$$= \rho_d + (\rho_b - \rho_d) \frac{(U_g - U_{mf})}{0.71\sqrt{gD_e} + (U_g - U_{mf})} \quad (40)$$

Integrating equation (40) and equation (35),

$$\begin{aligned} \bar{\rho}_{bed} &= \rho_d + (\rho_b - \rho_d) \frac{(U_g - U_{mf})}{0.71\sqrt{gD_e} + (U_g - U_{mf})} \\ &= \rho_p(1 - \varepsilon_{mf}) + \rho_g \varepsilon_{mf} + (\rho_g - \rho_p(1 - \varepsilon_{mf}) - \rho_g \varepsilon_{mf}) \frac{(U_g - U_{mf})}{0.71\sqrt{gD_e} + (U_g - U_{mf})} \\ &= (1 - \varepsilon_{mf})(\rho_p - \rho_g) \left(1 - \frac{(U_g - U_{mf})}{0.71\sqrt{gD_e} + (U_g - U_{mf})}\right) + \rho_g \end{aligned} \quad (41)$$

where D_e can be calculated using equation (15), which is

$$D_e = \phi(U - U_{mf})^{0.252} (h + 4A_D^{0.5})^{0.759} / 1.2 \quad (15)$$

where

$$\phi = \begin{cases} 0.252 & \text{for Geldart B type of particles} \\ & \text{(magnetite and sand (150 - 300}\mu\text{m))} \\ 0.153 & \text{for Geldart A type of particles} \\ & \text{(magnetite and sand (150 - 300}\mu\text{m))} \end{cases}$$

ε_{mf} can be calculated using equation (36), which is

$$\varepsilon_{mf} = \frac{H_{mf} - H_0}{H_0} \quad (33)$$

The minimum fluidization velocity of binary fluidization can be calculated using the correlation of Noda et al. by the modification of the equation of Wen and Yu which is:

$$A_r = A Re_{mf}^2 + B Re_{mf} \quad (8)$$

where

$$A_r = d^3 \rho_g (\rho_f - \rho_g) \frac{g}{\mu^2} \quad (4)$$

$$Re_{mf} = \frac{d \rho_g \mu_{mf}}{\mu} \quad (5)$$

where A and B are constants.

Noda et al. determined these two parameters, which are given by

$$A = 36.2 \left(\frac{d_m \rho_f}{\bar{d} \rho_m} \right)^{-0.196} \quad (9)$$

$$B = 1397 \left(\frac{d_m \rho_f}{\bar{d} \rho_m} \right)^{0.296} \quad (10)$$

Therefore, once the minimum fluidization velocity is determined, the bed density of fluidized bed can be calculated using equations (38), (29) and (33).

3.4 Conclusions

Bubble dynamics and bed expansion of binary fluidization systems have been investigated experimentally using image process technology. The effect of the addition of light particles on bubble diameter, bubble velocity and bed expansion was obtained through the comparison between binary fluidization systems and single-component fluidization systems. The main conclusions are as follows:

- (i) The density of fluidized bed can be decreased significantly applying a binary fluidization system where lighter particles are added. In addition, the minimum fluidization velocity of binary mixtures can be reduced by the addition of lighter particles. The decrease of these two parameters can bring down the energy cost.
- (ii) Bubble diameter of binary mixtures is increasing with the distance above gas distributor and excess gas velocity, but decreasing with volume fraction of light particles, which means binary fluidization can give a good fluidization with small bubbles population and their homogeneous distribution.
- (iii) Bubble rise velocity is also increasing with the distance above gas distributor and excess gas velocity and decreasing with volume fraction of light particles.
- (iv) Binary fluidization systems are able to give bigger bed expansion compared to single-component systems, which indicates a high quality of fluidization with large number of small bubbles.

- (v) The correlation for estimation of bubble diameter for single-component fluidization systems was approved to be also able to give good prediction of bubble size of binary fluidization systems. In addition, a method for prediction of bed density of binary fluidization systems was also developed.
- (vi) Binary fluidization systems have the ability of controlling the bed densities and generating good fluidization environment. Therefore, binary fluidization system is a high-efficiency method in dry coal beneficiation and other industrial processes.

Nomenclature

A_b, A	Surface area of a single bubble, cm^2
A_D	The diameter of hole on the distributor, m
A_t	Cross-sectional area of the bed, cm
D_{BM}	The maximum bubble diameter, cm
D_{B0}	Initial bubble diameter, cm
D_t	Bed diameter, cm
d_p, d	Particle size, μm
D_e	Equivalent bubble diameter, cm
D, D_B	Bubble diameter, m
e	Bed expansion
F_b	The buoyant force, N
F_d	Drag force, N
g	Acceleration of gravity, m/s^2
H, h	Bed height (The distance above gas distributor), m
H_0	Initial bed height, m
H_e	Expanded bed height, m
Δt	Time interval between consecutive frames, s
U	Superficial gas velocity, m/s
u	Velocity of fluid, m
u_b	Bubble rise velocity, cm/s
U_{mf}	The minimum fluidization velocity, cm/s

V_b	Bubble volume, cm ³
w	Bed width, cm
x_i	Abscissa of bubble center, cm
y_i, y_{i-1}	Ordinate of bubble center, cm
ρ_p	The density of particles, kg/m ³
ρ_g	The density of fluidizing gas, kg/m ³
ρ_f	The density of fluidizing medium, kg/m ³
μ	Viscosity of fluidizing gas, Pa.s

Greek letters

ρ

μ

Reference

Andreux, R. and J. Chaouki (2005), Behaviors of the bubble, cloud, and emulsion phases in a fluidized bed, *AIChE Journal* 54: 406-414.

Busciglio, A., Vella, G. and G. Micale (2012), On the bubbling dynamics of binary mixtures of powders in 2D gas-solid fluidized beds, *Powder Technology* 231: 21-34.

Coltters, R. and A.L. Rivas (2004), Minimum fluidization velocity correlations in particulate systems, *Powder Technology* 147 (1-3): 34-48.

Darton, R. C., LaNAUZE, R. D., Davidson, J. F. and D. Harrison (1977), Bubble growth due to coalescence in fluidized beds, *Trans. Inst. ChemE* 55: 274-280.

Davidson, J. F. and D. Harrison (1963), *Fluidized particles*, Cambridge university press.

Whitehead, A.B., Dent, D.C. and G.N. Bhat (1967), Fluidization studies in large gas-solid systems-Part 1: bubble rise rates, *Powder Technology* 1: 143-148.

Dwari, R. K. and K. H. Rao (2007), Dry beneficiation of coal-A review, *Mineral processing & extractive metallurgy review* 28 (3): 177-234.

Geldart, D. (1972), The size and frequency of bubbles in two and three dimensional gas fluidized beds, *Powder Technology* 4: 41-45.

Halow, J. S., Fasching, G. E., Nicoletti, P. and J. L. Spenik (1993), Observation of a fluidized bed using capacitance imaging, *Chemical Engineering Science* 48: 643-659.

Horio, M. and A. Nonaka (1987), A generalized bubble diameter correlation for gas-solid fluidized beds, *AIChE Journal* 33 (11): 1865-1872.

Kage, H., Yamaguchi, H., Ishii, H. and Y. Matsuno (1991), Bubble Behavior in Bubbling Fluidized Beds of Binary Particles, *Journal of Chemical Engineering of Japan* 24 (4): 525-531.

Lim, C., Glibertson, M. and A. Harrison (2007), Bubble distribution and behavior in bubbling fluidized beds, *Chemical Engineering Science* 62: 56-69.

McKeen, T. and T. Pugsley (2003), Simulation and experimental validation of a freely bubbling bed of FCC catalyst, *Powder Technology* 129: 139-152.

Mudde, R.F., Schulte, H.B.M. and H.E.A. van den Akker (1994), Analysis of a bubbling 2-D gas-fluidized bed using image processing, *Powder Technology* 81: 149-159.

Mori, S. and C. Y. Wen (1975), Estimation of bubble diameter in gaseous fluidized beds, *AIChE*

Journal 21(1): 109-115.

Narsimhan, G. (1965), On a generalized expression for prediction of minimum fluidization velocity, *AIChE Journal* 11 (3): 550-554.

Noda, K., Uchida, S., Makino, T. and H. Kamo (1986), Minimum fluidization velocity of binary mixture of particles with large size ratio, *Powder Technology* 46 (2-3): 149-154.

Park, W. H. and W. K. Kang (1969), The properties of bubbles in fluidized beds of conducting particles as measured by an electroresistivity probe, *Chemical Engineering Science* 24: 851-865.

Rowe, P. N. and B. A. Partridge (1965), An X-ray study of bubbles in fluidized beds, *Institution of Chemical Engineers* 43: 157-175.

Van Houwelingen, J. A. and T. P. R. de Jong (2004), Automatic sorting and control in solid fuel processing: Opportunities in European perspective, *Geologica Belgica* 7 (3-4): 334-343.

Werther, J. and O. Molerus (1973), The local structure of gas fluidized beds —I. A statistically based measuring system, *International Journal of Multiphase Flow* 1 (1): 103-122.

Wen, C.Y. and Y.H. Yu (1966), A generalized method for predicting the minimum fluidization velocity, *AIChE Journal* 12 (3): 610-612.

Werther, J. (1978), Effect of gas distributor on the hydrodynamics of gas fluidized beds, *Ger. Chem. Eng.* 1: 166-174.

Yasui, George and L. N. Johanson (1958), Characteristics of gas pockets in fluidized beds, *AIChE Journal* 4 (4): 445-452.

Chapter 4 General conclusions

Gas-solid fluidization has been approved to be an environmental friendly approach in dry coal beneficiation. The effects of bubble behaviors on the quality of fluidization are significant. In the first part, bubble dynamics of four different particles (including magnetite powder, sand particles and FCC catalyst) covering the range of 75 μm to 300 μm in a 2D fluidized bed have been studied using image processing technology. In addition, bed expansion as a parameter indicating the amount of bubble phase has also been analyzed. The two-dimensional fluidized bed is able to give detail observation of bubble behaviour due to its small thickness. These parameters involved in bubble dynamics are the minimum fluidization velocity, bubble size and bubble velocity. The results show that magnetite powder has the largest minimum fluidization velocity, while FCC catalyst is in possession of the smallest minimum fluidization velocity. In terms of bubble size and bubble rise velocity, Geldart B type particles (magnetite powder and sand particles (150-300 μm)) have bigger bubble size and bubble rise velocity than Geldart A type of particles (sand particles (75-125 μm) and FCC catalyst). In addition, bubble size and bubble rise velocity are also increasing with the distance above the gas distributor, excess gas velocity and particle size. Bubble rise velocity is dominated by bubble size due to the forces exerted on bubbles. Given the equation for estimation of bubble diameter (Darton et al. 1977) excludes the effect of particles size and bubble splitting on bubble diameter, a new improved correlation for prediction of bubble diameter was proposed as follows:

$$D_e = \phi(U - U_{mf})^{0.2036} (h + 4A_D^{0.5})^{0.7591} / 1.2$$

where

$$\phi = \begin{cases} 0.2522 & \text{for Geldart B type of particles} \\ & \text{(magnetite and sand (150 – 300}\mu\text{m))} \\ 0.1529 & \text{for Geldart A type of particles} \\ & \text{(magnetite and sand (150 – 300}\mu\text{m))} \end{cases}$$

According to the comparison between experimental data from other researchers' work and predicted values using this equation, the new correlation for bubble size is capable of giving a better prediction of bubble diameter.

Bed expansion as a significant parameter for determining the amount of bubble phase was also studied experimentally. In this work, direct observation of bed expansion and bed expansion induced by pressure drop were applied for analysis. The results show that Geldart A type particles (FCC catalyst and sand particles (75-125 μm)) tend to have a bigger bed expansion than Geldart B type particles (magnetite powder and sand particles (150-300 μm)), which means larger bubble population of Geldart A type of particles. Theoretical and experimental determination of bed expansion showed the same pattern.

The second part of the experiments was designed to investigate bubble dynamics and bed expansion in binary systems. The binary mixtures used as the medium solids can lower the bed density significantly compared to the adjustments by gas velocity. Four binary mixtures with different compositions of volume fraction of light sand particles were considered. A comprehensive comparison of the minimum fluidization velocity, bubble size, bubble rise velocity and bed expansion between binary fluidization systems and single-component system was accomplished. The results show that the minimum fluidization velocity of binary mixture is decreasing with increasing volume fraction of light (sand) particles. The comparison of bubble size illustrates that magnetite powder has the largest minimum fluidization velocity, while sand particles have the smallest value in the range of parameters used in this study. As

for bubble size and bubble rise velocity, magnetite powder still has the largest value, while sand particles have the smallest and binary mixtures' bubble diameter and bubble rise velocity fall in between. Moreover, bubble size and bubble rise velocity have the same growth pattern with bed height, excess gas velocity and volume fraction of sand particles. The proposed correlation for estimation of bubble diameter for single-component fluidization systems was verified to provide a good prediction of bubble diameter for binary fluidization systems. In addition, the bed expansion of binary mixtures increases with the volume fraction of lighter (sand) particles. In brief, the addition of light sand particles can give smaller minimum fluidization velocity, smaller bubble size and bubble rise velocity but bigger bed expansion, which means that binary fluidization can provide higher quality of fluidization for dry coal beneficiation and other industrial processes. A method for estimation of bed density for single-component fluidization systems and binary fluidization systems was developed based on the new correlation of bubble diameter proposed.

Reference

Andreux, R. and J. Chaouki (2005), Behaviors of the bubble, cloud, and emulsion phases in a fluidized bed, *AIChE Journal* 54: 406-414.

Busciglio, A., Vella, G. and G. Micale (2012), On the bubbling dynamics of binary mixtures of powders in 2D gas-solid fluidized beds, *Powder Technology* 231: 21-34.

Busciglio, A., Vella, G., Micale, G. and L. Rizzuti (2010), Experimental analysis of bubble size distribution in 2D gas fluidized beds, *Chemical Engineering Science* 65: 4782-4791.

BP Statistical Review of World Energy 2016, BP, London 2016.

Beeckmans, J. M. and T. Minh (1977), Separation of mixed granular solids using the fluidized counter-current cascade principle, *The Canadian Journal of Chemical Engineering* 55: 493-496.

Chen Q. R. and Y. F. Yang(1994), Development of dry beneficiation of coal in China, *Coal preparation* 23: 3-12.

Coltters, R. and A.L. Rivas (2004), Minimum fluidization velocity correlations in particulate systems, *Powder Technology* 147 (1-3): 34-48.

Douglas, E. and T. Walsh (1966), New type of dry heavy medium gravity separator, *Transactions of the Institute of Mining and Metallurgy* 75C: 226–232.

Darton, R. C., LaNAUZE, R. D., Davidson, J. F. and D. Harrison (1977), Bubble growth due to coalescence in fluidized beds, *Trans. Inst. ChemE* 55: 274-280.

Davidson, J. F. and D. Harrison (1963), *Fluidized particles*, Cambridge university press.

Whitehead, A.B., Dent, D.C. and G.N. Bhat (1967), Fluidization studies in large gas-solid systems-Part 1: bubble rise rates, *Powder Technology* 1: 143-148.

Dwari, R. K. and K. H. Rao (2007), Dry beneficiation of coal-A review, *Mineral processing & extractive metallurgy review* 28 (3): 177-234.

Fraser, J. and H. F. Yancey (1926), Artificial storm of air-sand floats coal on its upper surface, leaving refuse to sink, *Coal Age* 29: 325-327.

Geldart, D. (1972), The size and frequency of bubbles in two and three dimensional gas fluidized beds, *Powder Technology* 4: 41-45.

Halow, J. S., Fasching, G. E., Nicoletti, P. and J. L. Spenik (1993), Observation of a fluidized

bed using capacitance imaging, *Chemical Engineering Science* 48: 643-659.

Horio, M. and A. Nonaka (1987), A generalized bubble diameter correlation for gas-solid fluidized beds, *AIChE Journal* 33 (11): 1865-1872.

Kage, H., Yamaguchi, H., Ishii, H. and Y. Matsuno (1991), Bubble Behavior in Bubbling Fluidized Beds of Binary Particles, *Journal of Chemical Engineering of Japan* 24 (4): 525-531.

Lim, C., Glibertson, M. and A. Harrison (2007), Bubble distribution and behavior in bubbling fluidized beds, *Chemical Engineering Science* 62: 56-69.

Lim, K. and P. Agarwal (1990), Conversion of pierced lengths measured at a probe to bubble size measures: an assessment of the geometrical probability approach and bubble shape models, *Powder Technology* 63: 205-219.

Lohn, P. (1971), Fluidized bed heavy medium separation-A modern dry separation procedure, *Aufbereitung Technik* 3: 140-146.

McKeen, T. and T. Pugsley (2003), Simulation and experimental validation of a freely bubbling bed of FCC catalyst, *Powder Technology* 129: 139-152.

Mudde, R.F., Schulte, H.B.M. and H.E.A. van den Akker (1994), Analysis of a bubbling 2-D gas-fluidized bed using image processing, *Powder Technology* 81: 149-159.

Mori, S. and C. Y. Wen (1975), Estimation of bubble diameter in gaseous fluidized beds, *AIChE Journal* 21(1): 109-115.

Ma, J., Liu, D. and X. Chen (2015), Bubble behaviors of large cohesive particles in a 2D fluidized bed, *Ind. Eng. Chem. Res.* 55: 624-634.

Narsimhan, G. (1965), On a generalized expression for prediction of minimum fluidization velocity, *AIChE Journal* 11 (3): 550-554.

Noda, K., Uchida, S., Makino, T. and H. Kamo (1986), Minimum fluidization velocity of binary mixture of particles with large size ratio, *Powder Technology* 46 (2-3): 149-154.

Park, W. H. and W. K. Kang (1969), The properties of bubbles in fluidized beds of conducting particles as measured by an electroresistivity probe, *Chemical Engineering Science* 24: 851-865.

Rowe, P. N. and B. A. Partridge (1965), An X-ray study of bubbles in fluidized beds, *Institution of Chemical Engineers* 43: 157-175.

Rowe, P.N. and C.X.R. Yacono (1976), The bubbling behaviour of fine powders when fluidized,

Chemical Engineering Science 31: 1179-1192.

Sahu, A. K., Biswal, S. K. and A. Parida (2009), Development of air dense medium fluidized bed technology for dry beneficiation of coal – A review, *International Journal of Coal Preparation and Utilization* 29 (4): 216-241.

Van Houwelingen, J. A. and T. P. R. de Jong (2004), Automatic sorting and control in solid fuel processing: Opportunities in European perspective, *Geologica Belgica* 7 (3-4): 334-343.

Verma, V. and T.P. Johan (2014), Bubble dynamics in a 3-D gas–solid fluidized bed using ultrafast electron beam X-ray tomography and two-fluid model, *AIChE Journal* 60 (5): 1632-1644.

Werther, J. and O. Molerus (1973), The local structure of gas fluidized beds —I. A statistically based measuring system, *International Journal of Multiphase Flow* 1 (1): 103-122.

Wen, C.Y. and Y.H. Yu (1966), A generalized method for predicting the minimum fluidization velocity, *AIChE Journal* 12 (3): 610-612.

Werther, J. (1978), Effect of gas distributor on the hydrodynamics of gas fluidized beds, *Ger. Chem. Eng.* 1: 166-174.

Werther, J. (1974), Influence of the bed diameter on the hydrodynamics of gas fluidized beds, *AIChE Symp. Ser.* 70 (141): 53-62.

Whitehead, A.B., Dent, D.C. and G.N. Bhat (1967), Fluidization studies in large gas-solid systems-Part 1: bubble rise rates, *Powder Technology* 1: 143-148.

Xuliang Yang, Yuemin Zhao and Zhenfu Luo (2016), Dry cleaning of fine coal based on gas-solid two-phase flow: A review, *Chemical Engineering Technology* 40(3): 439-449.

Yasui, George and L. N. Johanson (1958), Characteristics of gas pockets in fluidized beds, *AIChE Journal* 4 (4): 445-452.

Curriculum Vitae

Name:

Bowen Han

Post-secondary Education and Degrees:

2012-2016 B.E. Tianjin University, Tianjin, China

2015-2016 Exchange Student Western University, London, Ontario, Canada

2016-2017 M.E.Sc Western University, London, Ontario, Canada